

1 Potential impact of carbonaceous aerosol on the Upper Troposphere and Lower  
2 Stratosphere (UTLS) and precipitation during Asian summer monsoon in a  
3 global model simulation

4 Suvarna Fadnavis<sup>1</sup>, Gayatry Kalita<sup>1</sup>, K. Ravi Kumar<sup>1</sup>, Blaz Gasparini<sup>2</sup> and Jui-Lin Frank Li<sup>3</sup>

5 <sup>1</sup>Indian Institute of Tropical Meteorology, Pune, India

6 <sup>2</sup>Institute for Atmospheric and Climate Science, ETH Zürich, Switzerland

7 <sup>3</sup>Jet Propulsion Laboratory, California Institute of Technology, Pasadena, California

8 **Abstract**

9 Recent satellite observations show efficient vertical transport of Asian pollutants from the  
10 surface to the upper level anticyclone by deep monsoon convection. In this paper, we  
11 examine the transport of carbonaceous aerosols including Black Carbon (BC) and Organic  
12 Carbon (OC) into the monsoon anticyclone using of ECHAM6-HAM, a global aerosol  
13 climate model. Further, we investigate impacts of enhanced (doubled) carbonaceous aerosols  
14 emissions on the UTLS, underneath monsoon circulation and precipitation from sensitivity  
15 simulations.

16 These model simulations show that boundary layer aerosols are transported into the monsoon  
17 anticyclone by the strong monsoon convection from the Bay of Bengal, southern slopes of  
18 the Himalayas and the South China Sea. Doubling of emissions of BC and OC aerosols, each,  
19 over the South East Asia (10°S - 50°N; 65°E - 155°E) show that lofted aerosols produces  
20 significant warming (0.6K - 1K) over the Tibetan Plateau (TP) near 400 hPa – 200 hPa and  
21 instability in the mid/upper troposphere. They enhance radiative heating rates (0.02 K day<sup>-1</sup> -  
22 0.03 K day<sup>-1</sup>) near the tropopause. The enhanced carbonaceous aerosols alter aerosol

23 Radiative Forcing (RF) at the surface by  $-4.74 \pm 1.42 \text{ W m}^{-2}$ ; at the Top Of the Atmosphere  
24 (TOA) by  $+0.37 \pm 0.26 \text{ W m}^{-2}$  and in the atmosphere by  $+5.11 \pm 0.83 \text{ W m}^{-2}$  over the TP and  
25 Indo Gangetic Plains region ( $15^{\circ}\text{N} - 35^{\circ}\text{N}$ ,  $80^{\circ}\text{E} - 110^{\circ}\text{E}$ ). Atmospheric warming increases  
26 vertical velocities and thereby cloud ice in the upper troposphere. An anomalous warming  
27 over the TP facilitates the relative strengthening of the monsoon Hadley circulation and  
28 increases moisture inflow by strengthening the cross-equatorial monsoon jet. This increases  
29 precipitation amounts over India ( $1 \text{ mm day}^{-1} - 4 \text{ mm day}^{-1}$ ) and eastern China ( $0.2 \text{ mm day}^{-1} -$   
30  $2 \text{ mm day}^{-1}$ ). These results are significant at 99 % confidence level.

31 *Key words:* Aerosol radiative forcing; Black Carbon and Organic Carbon aerosols;  
32 ECHAM6-HAM; Upper Troposphere and Lower Stratosphere (UTLS); Asian Tropopause  
33 Aerosol Layer (ATAL).

34

## 1. Introduction

South East Asia (10°S – 50°N; 65°E – 155°E) is one of the most fast-growing regions in terms of population and economy which contributes significantly to the emission of global aerosol particles (Ramanathan and Crutzen, 2003; Lin et al., 2013). India and China are the two main contributors in Asia (Carmichael et al., 2009; Lin et al., 2014; Butt et al., 2016). Black Carbon (BC) and Organic Carbon (OC) are the important aerosol species as they substantially contribute to the climate forcing (Penner et al., 1998; Chung and Seinfeld, 2002; Ramanathan and Carmichael, 2008; Hodnebrog et al., 2014); alter the energy balance in the atmosphere and the global water cycle (Solomon et al., 2007). Recent studies show that their impacts on local meteorology and monsoon circulation are large (Ackerman et al., 2000; Ramanathan et al., 2001a, 2001b; Lelieveld et al., 2001; Menon et al., 2002; Manoj et al., 2011). BC and OC together account for more than 60% of the Aerosol Optical Depth (AOD) (Chin et al., 2009; Streets et al., 2009).

There is ever growing concern for rapidly increasing anthropogenic emissions of carbonaceous aerosols namely BC and OC. Global emissions of BC have almost doubled during the past century (Baron et al., 2009). Developing countries in Asia, e.g. India and China produce BC emissions at high growth rates. These countries together produced about 40% of total world BC emissions from combustion (Kopp and Mauzerall, 2010). The estimated growth of BC is 46% (33% in OC) over China and 41% (35% in OC) over India during 2000 to 2010 (Lu et al., 2011). On a regional scale, their emissions are high over densely populated Indo-Gangetic Plains in India and eastern China (Kumar et al., 2011; Lelieveld, 2001; Gautam et al., 2011; Fadnavis et al., 2013; Zhang et al., 2015). Over the Asian region, (Indo-Gangetic Plains and north-eastern China) emission of OC is almost twice as that of BC (Fig. 1).

59 The majority of BC and OC aerosols are formed by incomplete combustion (Satheesh and  
60 Ramanathan; 2000; Carmichael et al., 2009). The important emission sources of BC aerosols are  
61 diesel vehicles, exhaust from coal-based power plants, exhaust from industries, forest fires and  
62 residential bio-fuel and fossil-fuel combustion. The OC aerosols are emitted from fossil fuel and  
63 biofuel burning and natural biogenic emissions. Biogenic carbonaceous aerosol are produced  
64 from of plant debris, pollen, fungal spores, and bacteria (Jacobson et al., 2000; Bond et al., 2004)  
65 and secondary organic aerosol from the oxidation of volatile organic compounds (VOCs)  
66 (Solomon et al., 2007).

67 Recent satellites, Cloud Aerosol Lidar and Infrared Path finder Satellite Observation  
68 (CALIPSO) (Vernier et al., 2011; Thomason and Vernier, 2013), Stratospheric Aerosol and Gas  
69 Experiment II (SAGE) (Thomason and Vernier, 2013) and Balloonsonde (Vernier, et al., 2015)  
70 observations show Asian Tropopause Aerosol Layer (ATAL) near the tropopause persisting  
71 during the monsoon season (June-September). Satellite observations reveal transport of trace  
72 gasses (CO, PAN, H<sub>2</sub>O HCN) into the upper level monsoon anticyclone by deep monsoon  
73 convection (Park et al., 2009; Randel et al., 2010, Kunze et al.,2010; Ploeger et al., 2011; 2012;  
74 2013; Fadnavis et al., 2014; 2015, Govardhan et al., 2017). Moreover, both back trajectory  
75 analysis based on CALIOP observations (Vernier et al., 2015) and modeling studies (Fadnavis et  
76 al., 2013) indicate that deep monsoon convection transports boundary layer aerosols into the  
77 UTLS. A Civil Aircraft for Regular Investigation of atmosphere Based on an Instrument  
78 Container (CARBIC) measurements show aerosols at the lower levels in the ATAL contain  
79 higher levels of carbonaceous and sulfate aerosols. The ratio of carbon to sulfur is ~4.0 with  
80 concentrations of carbon ~36 ng/m<sup>3</sup> and sulfur ~ 13 ng/m<sup>3</sup> in the Asian upper troposphere during  
81 August 2006, 2007 and 2008 (Vernier et al., 2015). Carbonaceous aerosols in the upper

82 troposphere lead to atmospheric heating due to their absorptive properties which may  
83 subsequently alter the atmospheric thermal structure and cloud amounts. Higher concentrations  
84 of carbonaceous aerosols in the ATAL may significantly alter thermal structure of the UTLS and  
85 therefore the underneath monsoon circulation (Meehl et al., 2008; Kloster et al., 2009). The  
86 ATAL may affect the Radiative Forcing (RF) regionally. Vernier et al., (2015) reported that the  
87 ATAL had exerted a short-term regional forcing at the top of the atmosphere  $\sim -0.1 \text{ W/m}^2$  during  
88 past two decades.

89 BC and OC aerosols absorb and scatter radiation, resulting in heating of the atmosphere and a  
90 layer of aerosols in the UTLS may reduce solar radiation reaching the Earth's surface (Penner et  
91 al., 1998). The global mean estimated cumulative (since 1970) BC radiative effect is  $+0.3 \text{ W/m}^2$   
92 while OC emitted from fossil fuels is estimated to be  $-0.1 \text{ W/m}^2$  (Myhre et al., 2013). The  
93 presence of BC aerosols can change the sign of forcing from negative to positive (Haywood and  
94 Shine, 1997). Studies pertaining to BC/OC RF are sparse over the Indian region. Sreekanth et al.,  
95 (2007) reported BC RF at the TOA  $+2.36 \text{ W/m}^2$  and  $-9.9 \text{ W/m}^2$  at the surface at Visakhapatnam  
96 ( $17.7^\circ\text{N}$ ,  $83.3^\circ\text{E}$ ) during the monsoon season 2006. Babu et al., (2002) obtained BC RF  $+5 \text{ W/m}^2$   
97 at the TOA and at the surface  $-23 \text{ W/m}^2$  at Bangalore ( $13^\circ\text{N}$ ,  $77^\circ\text{E}$ ), during November-December  
98 2001. Badarinath and Latha, (2006) reported BC RF of  $+9 \text{ W/m}^2$  at the TOA and  $-33 \text{ W/m}^2$  at the  
99 surface at Hyderabad ( $78^\circ\text{E}$ ,  $17^\circ\text{N}$ ), India during January-May 2005.

100 Asian Summer Monsoon (ASM) has a major impact on agriculture, water resources, and  
101 economy and social life. Therefore it is important to study the impact of fast-growing Asian  
102 emission of carbonaceous aerosols on monsoon precipitation. However, there are a few studies  
103 reporting the impacts of carbonaceous aerosols on precipitation over India (Meehl et al., 2008;  
104 Wang et al., 2009; Ganguly et al., 2012) and China (Guo et al., 2013; 2015). Since convective

105 transport (during the monsoon season) inter-links tropospheric processes with the UTLS (Randel  
106 et al., 2010; Vogel et al., 2011, 2015; Fadnavis et al., 2013), it is essential to understand impacts  
107 of boundary layer emissions on the UTLS. To our knowledge, transport of carbonaceous aerosols  
108 from the boundary layer to upper troposphere, their impacts on the UTLS and connecting  
109 monsoon circulation are not explored in detail. In this study, we address the question of the  
110 impact of rapidly growing emissions of carbonaceous aerosols (BC and OC) on the thermal  
111 structure of the UTLS, monsoon transport processes and rainfall over India and China. We  
112 perform control and sensitivity simulations using the ECHAM6-HAM aerosol climate model. In  
113 sensitivity experiment, we have doubled anthropogenic emissions of BC and OC, each, over the  
114 South East Asia (10°S - 50°N; 65°E - 155°E). The paper is organized as follows; in Section 2  
115 model simulations and satellite observations are described. The transport processes are discussed  
116 in Section 3. The impact of enhanced carbonaceous aerosols emissions on the UTLS and  
117 monsoon precipitation are described in Section 4, followed by conclusions given in Section 5.

118

## 119 **2. Model simulations and satellite data analysis**

### 120 **2.1 Experimental setup and model simulations**

121 The fully coupled aerosol-climate model ECHAM6-HAM (version echam6.1.0-ham2.1-  
122 moz0.8) used in this study comprises the general circulation model ECHAM6 (Stevens et al.,  
123 2013) coupled to the aerosol sub-module Hamburg Aerosol Model (HAM) (Stier et al., 2005,  
124 Zhang et al., 2012). HAM predicts the evolution of sulfate (SU), black carbon (BC), particulate  
125 organic matter (POM), sea salt (SS), and mineral dust (DU) aerosols. The size distribution of  
126 aerosol population being described by seven log-normal modes with prescribed variance as in the  
127 M7 aerosol module (Vignati et al., 2004; Stier et al., 2005; Zhang et al., 2012). Moreover, HAM

128 uses the two-moment cloud microphysics scheme in which the nucleation scavenging of aerosol  
129 particles by acting as cloud condensation nuclei or ice nuclei, freezing and evaporation of cloud  
130 droplets and melting and sublimation of ice crystals is treated explicitly (Lohmann et al., 2010,  
131 Neubauer et al., 2014). The anthropogenic and fire emissions of SO<sub>2</sub>, BC, and OC are based on  
132 the AEROCOM-ACCMIP-II emission inventory. The anthropogenic emissions are based on  
133 Lamarque et al., (2010). The biomass burning emissions are from GICC 1850 -1950 (Mieville et  
134 al., 2010), RETRO 1960-1990 (Schultz et al., 2008) and GFED v2 (1997 - 2008) (van der Werf  
135 et al., 2006). Biogenic emissions are derived from MEGAN (Guenther et al., 1995), and fossil  
136 fuel sources are provided by the ACCMIP inventory (Lamarque et al., 2010). In the model,  
137 biogenic OC is directly inserted via emissions. Secondary organic aerosol (SOA) emissions are  
138 as described by Dentener et al. (2006). The emissions of sea salt (Guelle et al., 2001 and Stier et  
139 al., 2005) and dust (Tegen et al., 2002; Cheng et al., 2008) are computed interactively.

140         The model simulations are performed at the spectral resolution of T63. This spectral  
141 representation is associated with a horizontal resolution of 1.875° x 1.875° on a Gaussian grid and  
142 a vertical resolution of 47 levels spanning from the surface up to 0.01 hPa. The simulations have  
143 been carried out at a time step of 20 minutes. AMIP sea surface temperature (SST) and sea ice  
144 cover (SIC) are used as lower boundary conditions. Note that our base year for aerosol and trace  
145 gas emissions is 2000. Each simulation was performed for the 30 years from January 1979 to  
146 December 2009. We analyze simulated data for 20 years (1989 - 2009) considering initial ten  
147 years as spin-up time. Emissions are the same in each simulation, and meteorology varied  
148 because of different monthly sea surface temperature (SST) and sea ice (SIC) data. The  
149 interactive aerosols change the meteorology and feedback to aerosols variations. Most of the  
150 models underestimate BC and OC mass concentrations observed over Asia (Bond et al., 2013;

151 Butt et al., 2016; Winiger et al., 2016). Bond et al. (2013) have suggested that global atmospheric  
152 absorption attributable to black carbon is too low in many models and should be increased by a  
153 factor of three. Butt et al. (2016) obtained better predictions when residential carbonaceous  
154 emissions were doubled. We performed control experiment (CTRL) with baseline emissions (for  
155 the year 2000) and three sensitivity simulations for doubling of carbonaceous aerosols over the  
156 Asian region; (1) Demiss in which emissions of BC and OC, both, are doubled, (2) emissions of  
157 only BC aerosols are doubled in DBConly, and (3) simulation of doubling of only OC aerosols  
158 refers to DOConly. We compare CTRL simulation with Demiss scenario to analyze the impacts  
159 of doubled carbonaceous emissions (BC and OC together) on the UTLS and rainfall during ASM  
160 season (June - September). We also provide contribution of BC and OC aerosols separately from  
161 comparison of CTRL with DBConly and DOConly simulations.

## 162 **2.2 Satellite measurements**

### 163 **2.2.1 The Tropical Rainfall Measuring Mission (TRMM)**

164 The Tropical Rainfall Measuring Mission (TRMM) is a joint National Aeronautics and  
165 Space Administration (NASA) - Japan Aerospace Exploration (JAXA) satellite mission to  
166 monitor the tropical and subtropical precipitation and estimate its associated latent heat. TRMM  
167 was launched in 1997 from Tanegashima space center in Japan. The rainfall measuring  
168 instruments on the TRMM satellite include an electronically scanning radar Precipitation Radar  
169 (PR), (operating at 13.6 GHz), TRMM microwave image (TMI), a 9 channel passive microwave  
170 radiometer (which records radiation at the 10.65, 19.35, 37.0, 85.5 (V and H) and 21.3 (V) GHz),  
171 and Visible and Infrared Scanner (VIRS) with five operating channels (Kummerow et al., 1998).  
172 The 3B42 algorithm produces TRMM adjusted merged infrared precipitation rate and root mean  
173 square (RMS) precipitation error estimates (Huffman et al., 2007). The algorithm combines



174 multiple independent precipitation estimates from the TMI, Advanced Microwave Scanning  
175 Radiometer for Earth Observing Systems (AMSR-E), Special Sensor Microwave Imager (SSM/I),  
176 Special Sensor Microwave Imager/Sounder (SSMIS), Advanced Microwave Sounding Unit  
177 (AMSU), Microwave Humidity Sounder (MHS), and microwave-adjusted merged geo-infrared  
178 (IR). The final 3B42 precipitation (in mm hr<sup>-1</sup>) estimates have a 3-hourly temporal resolution and  
179 a 0.25-degree by 0.25-degree spatial resolution. TRMM precipitation can be obtained from  
180 [https://disc2.gesdisc.eosdis.nasa.gov/data/TRMM\\_L3/TRMM\\_3B42.7/](https://disc2.gesdisc.eosdis.nasa.gov/data/TRMM_L3/TRMM_3B42.7/). 3-hourly precipitation  
181 data are averaged to obtain daily mean. Then, seasonal mean (June-September) is computed from  
182 daily mean data. Further, seasonal mean data is averaged for 20 years (1997-2016) to obtain  
183 climatology of the monsoon season.

## 184 **2.2.2 CloudSat and Cloud-Aerosol Lidar Infrared Pathfinder Satellite Observations** 185 **(CALIPSO)**

186 Cloud–Aerosol Lidar and Infrared Pathfinder Satellite Observation (CALIPSO) and  
187 CloudSat are two A-Train constellation satellites, launched together in April 2006. They provide  
188 information related to the role of cloud and aerosol in the Earth's climate system and radiative  
189 imbalance of the atmosphere. The Cloud Profiling Radar (CPR) on board of CloudSat satellite is  
190 a 94-GHz nadir-looking radar which measures the power backscattered by clouds as a function  
191 of distance. It provides information on cloud abundance, distribution, structure, and radiative  
192 properties (Stephens et al., 2008). The Cloud-Aerosol Lidar with Orthogonal Polarization  
193 (CALIOP) is an elastically backscattered active polarization sensitive Lidar instrument onboard  
194 CALIPSO. The CALIOP transmit laser light simultaneously at 532 nm and 1064 nm at a pulse  
195 repetition rate 20.16Hz. The Lidar receiver subsystem measures backscatter intensity at 1064 nm  
196 and two orthogonally polarized components of 532 nm backscatter signal that provides the

197 information on the vertical distribution of aerosols and clouds, cloud particle phase, and  
198 classification of aerosol size (Winker et al., 2010; Powel et. al., 2013). In this study, we use Ice  
199 water content (IWC) dataset from the combined measurement of CloudSat and Calipso (2C-  
200 ICE\_L3\_V01) for the period 2007-2010. The 2C-ICE cloud product is an ice cloud retrieval  
201 derived from the combination of the CloudSat radar and CALIPSO Lidar, using a variational  
202 method for retrieving profiles of the IWC in ice clouds (Deng et al., 2013). The details of the  
203 data retrieval method are explained in Li et al., (2012). IWC data has been averaged for the  
204 monsoon season and period 2007 - 2010 to obtained seasonal climatology.

### 205 **2.3 Comparison with in-situ measurements**

206 We compare CTRL simulated BC concentrations with (1) aircraft measurements at  
207 Guwahati (26°11'N, 91°44'E) on 30August, 4 and 6 September 2009 from Rahul et al. (2014)  
208 and (2) Balloon borne measurements at Hyderabad (17°48' N; 78°40'E) (aethalometer installed  
209 on the hydrogen-inflated balloon) on 17 March 2010 from Babu et al., (2011). The model is not  
210 forced with meteorology therefore daily variations are not reproduced. Hence for comparison,  
211 monthly mean simulated BC concentrations are extracted at the grid centred at Guwahati and  
212 Hyderabad. Figure 2a-d shows the comparative analysis of model simulated BC and in-situ  
213 measurements. It can be seen that model underestimates BC emissions; therefore, we compare  
214 in-situ measurements with Demiss simulations, additionally. The profiles of BC concentration  
215 obtained from Demiss simulation show reasonable agreement with observations at Guwahati in  
216 the lower troposphere below 3km while differences are large between 3-6 km. Simulated BC  
217 profiles (CTRL and Demiss, both) show large differences with observations at Hyderabad  
218 (Fig.2d).These balloon-borne measurements show a variation of BC between 1000-10000 ng m<sup>-3</sup>  
219 from surface to 8.5 km while simulated BC concentration varies between 3000-2 ng m<sup>-3</sup> for the

220 same altitudes. The differences between in-situ measurements (balloon borne and aircraft) and  
221 model simulations may be due to number of factors such as the uncertainty in BC emissions in  
222 the model's emission inventory, uncertainty in the model's transport processes, and its coarse  
223 spatial grid ( $1.875^\circ \times 1.875^\circ$ ) compared to point measurement. Moreover, the meteorological  
224 conditions of each individual measurement day cannot be captured by monthly average values  
225 from the model output. The large differences at Hyderabad may be due to uncertainty in  
226 measurements due to attachment of aethalometer to the balloon. Although there are differences  
227 in the troposphere, Demiss simulations show reasonable agreement with measurements near the  
228 surface at Guwahati (Fig.2a-c) and Hyderabad (Fig. 2d). A similar agreement is also observed  
229 with observations near the surface (0-2km) at Kanpur ( $80^\circ 20'E$ ,  $26^\circ 26'N$ ) (Tripathi et al., 2007).  
230 The BC concentrations at Kanpur obtained from Demiss simulations  $\sim 7.5 \mu\text{g m}^{-3}$  -  $3 \mu\text{g m}^{-3}$  are  
231 comparable with observations  $\sim 8 \mu\text{g m}^{-3}$  -  $4 \mu\text{g m}^{-3}$ .

232         Figures 2e and 2f show the vertical distribution of cloud ice obtained from CTRL  
233 simulation and climatology of the seasonal mean from combined measurement of CloudSat and  
234 CALIPSO (2C-ICE) (2007-2010) respectively, averaged for the monsoon season (June-  
235 September) and ASM region ( $60^\circ E$  -  $110^\circ E$ ;  $15^\circ N$  -  $40^\circ N$ ). It can be seen that simulated ( $3 \text{ mg/kg}$   
236 -  $10 \text{ mg/kg}$ ) and observed cloud ice ( $5 \text{ mg kg}^{-1}$  -  $17 \text{ mg kg}^{-1}$ ), both, show high amounts in the  
237 upper troposphere ( $450 \text{ hPa}$  -  $200 \text{ hPa}$ ) over the ASM region. The model simulations show  
238 maximum ( $7 \text{ mg kg}^{-1}$  -  $10 \text{ mg kg}^{-1}$ ) at  $\sim 350 \text{ hPa}$  -  $250 \text{ hPa}$  over  $80^\circ E$  -  $100^\circ E$  while satellite  
239 observations ( $12 \text{ mg kg}^{-1}$  -  $17 \text{ mg kg}^{-1}$ ) show it at  $\sim 450 \text{ hPa}$  -  $200 \text{ hPa}$  over  $\sim 80^\circ E$  -  $120^\circ E$ . These  
240 differences may be related to uncertainties in satellite observations (Deng et al., 2010) and model  
241 biases, e.g., the model does not consider large ice particles unlike the cloud ice measurement  
242 from CloudSat and CALIPSO. The total ice water mass estimate from 2C - ICE, combine

243 measurements from CALIPSO Lidar depolarization which is sensitive to small ice particle (i.e.,  
244 cloud ice represented in GCMs) while CloudSat radar which is very sensitive to larger ice  
245 particles (i.e., precipitating ice or snow). In most global climate models including all the CMIP3  
246 and most of the CMIP5, only small particles (i.e., cloud ice) are represented prognostically. The  
247 mass of large ice particles (about two-third of total ice) and their radiative effects, however, are  
248 not included (e.g., Li et al., 2012; 2013).

249 We compare simulated (CTRL) seasonal mean (June-September) precipitation with TRMM  
250 climatology (1997-2016). Figures 2g and 2h show the distribution of precipitation as obtained  
251 from CTRL simulation and TRMM respectively. It can be seen that general spatial pattern of  
252 precipitation simulated by the model is in good agreement with the TRMM. The model could  
253 reproduce high amounts of precipitation over the Bay of Bengal, the South China Sea, and the  
254 Western Ghats, in agreement with a numbers of past studies (Wang and Linho, 2002; Hirose and  
255 Nakamura, 2005; Xie et al., 2007; Takahashi, 2016). However, model underestimates the rainfall  
256 over northern India and the Western coast of India by  $\sim 2 \text{ mm day}^{-1}$  -  $10 \text{ mm day}^{-1}$  and  
257 overestimates over the Tibetan Plateau (TP) and the South China Sea by  $\sim 5 \text{ mm day}^{-1}$  -  $12 \text{ mm}$   
258  $\text{day}^{-1}$ . It may be related uncertainties in emissions, transport errors, and model coarse resolution.

259

### 260 **3. Transportation of aerosol to the UTLS**

261 Figure 3a depicts the vertical distribution of carbonaceous aerosols averaged over North  
262 India ( $75^{\circ}\text{E}$  -  $100^{\circ}\text{E}$ ;  $25^{\circ}\text{N}$  -  $45^{\circ}\text{N}$ ) during the annual cycle as obtained from CTRL simulation. It  
263 shows elevated levels of aerosols (BC and OC together) from the surface to the tropopause  
264 during pre-monsoon (March-May) and monsoon seasons. It also shows a layer of carbonaceous  
265 aerosols ( $\sim 5 \text{ ng m}^{-3}$ ) in the upper troposphere  $\sim 170 \text{ hPa}$  -  $100 \text{ hPa}$ . A layer of aerosols in the

266 upper troposphere is also observed by satellite (SAGE II, CALIPSO) and Lidar measurements  
267 during the monsoon season (Vernier et al., 2011; Thomason and Vernier, 2013; Fadnavis et al.  
268 2013; He et al., 2014). Over the TP this aerosol layer extends above the tropopause (18 km - 19  
269 km) (He et al., 2014).

270 A prominent feature in the UTLS over the ASM region during the summer season is a  
271 large anticyclone. Satellite observations show a persistent maximum in trace gases (CO, H<sub>2</sub>O,  
272 PAN, HCN, CH<sub>4</sub>, etc) (Li et al., 2005; Randel and Park 2006, Fu et al., 2006; Park et al., 2008;  
273 2009, Randel et al., 2010; Fadnavis et al., 2013, 2014, 2015) and aerosols (Tobo et. al., 2007;  
274 Vernier et al., 2011; Thomason and Vernier, 2013; Yu et al., 2015) in the ASM anticyclone.  
275 Figure 3b exhibits the distribution of seasonal (June-September) mean carbonaceous aerosols  
276 (BC and OC together) from CTRL simulation in the anticyclone (~100 hPa). In agreement with  
277 previous studies (Tobo et al., 2007 Vernier et al., 2011), Fig. 3b also shows confinement of high  
278 carbonaceous aerosols concentration (~5.5 ng m<sup>-3</sup>) within the anticyclone. The wind vector at  
279 100hPa depicts the extent of the anticyclone (20°E - 120°E and 15°N - 40°N).

280 Previous studies from model simulations and trajectory analysis show that rapid transport  
281 of trace gases and aerosols from Asian boundary layer into the anticyclone is closely linked with  
282 the deep ASM convection (Li et al, 2005; Randel and Park, 2006; Park et al., 2007; Park et al,  
283 2009; Xiong et al., 2009; Fadnavis et al, 2013, 2014 , 2015). We plot longitude-pressure and  
284 latitude-pressure cross sections of carbonaceous aerosol from CTRL simulations to understand  
285 their transport. Figure 3c displays seasonal mean longitude-pressure variation of carbonaceous  
286 averaged over 15°N - 35°N, along with wind vectors. It indicates that they are lifted up from the  
287 Bay of Bengal, Indo-Gangetic Plains (70°E - 90°E) and South China Sea (110°E - 130°E) into the  
288 anticyclone increasing the aerosol concentration to 4 ng m<sup>-3</sup> - 6 ng m<sup>-3</sup> in the UTLS (above

289 200hPa) across 40°E - 110°E. Transport from southern slopes of Himalaya is evident in Figs. 3d.  
290 The vertical distribution of both BC and OC show transport from above mentioned regions into  
291 the UTLS (Fig.S1). The amount of OC ( $3 \text{ ng m}^{-3}$  -  $4 \text{ ng m}^{-3}$ ) crossing the tropopause is higher  
292 than BC ( $0.8 \text{ ng m}^{-3}$  -  $1 \text{ ng m}^{-3}$ ). Figures 3e and 3f show the condensed cloud water (both liquid  
293 and ice). Its maxima point out areas of frequent deep convective activity over the Bay of Bengal  
294 and the South China Sea (Fig. 3e) and the southern flanks of the Himalayas (Fig. 3f). Thus  
295 transport of carbonaceous aerosols (seen in Figs. 3c and 3d) from these regions into the upper  
296 level anticyclone may be due to deep monsoon convection. Pollution transport (CO, HCN, NO<sub>x</sub>,  
297 PAN) from the Asian region to the UTLS due to monsoon convection is also reported by Park et  
298 al. (2007), Randel et al. (2010), Fadnavis et al., (2014, 2015). Figures 3c and 3d show that a  
299 fraction of aerosols crosses the tropopause and enters into the lower stratosphere. It may be due  
300 to large scale upward motion within the anticyclone. Recently, trajectory analysis showed that air  
301 masses within the anticyclone are transported into the lower stratosphere in the northern  
302 subtropics (Garny and Randel, 2016). We analyze the vertical profile of anomalies of  
303 carbonaceous aerosols obtained from a difference between Demiss and CTRL simulations.  
304 Longitude-pressure and latitude-pressure cross sections of the anomalies are shown in Figs. 4a  
305 and 4b respectively. Enhanced anomalies are seen along the transport pathways, e.g., from the  
306 Bay of Bengal, the South China Sea and southern flanks of the Himalayas into the anticyclone.  
307 They show an enhancement of nearly  $4 \text{ ng m}^{-3}$  relative mass of aerosol near the tropopause and  
308 part of it ( $>2 \text{ ng m}^{-3}$ ) enters the lower stratosphere. Comparisons of DBConly and DOConly  
309 simulations with CTRL show anomalies in BC  $3 \text{ ng m}^{-3}$  -  $5 \text{ ng m}^{-3}$  and OC  $8 \text{ ng m}^{-3}$  -  $12 \text{ ng m}^{-3}$  in  
310 the lower stratosphere (not shown).  
311

## 312 **4. Impact of enhanced carbonaceous aerosols emissions**

### 313 **4.1 Impact on radiative forcing and heating rates**

314 The convectively transported carbonaceous aerosols may alter RF, heating rates,  
315 temperature, and vertical velocities in the UTLS. The carbonaceous aerosol can affect the  
316 radiative energy balance of the atmosphere directly by scattering and absorbing solar radiation  
317 and indirectly by acting as cloud condensation nuclei (Rosenfield, 2000). Anomalies in aerosol  
318 RF estimated from Demiss, DBConly and DOConly simulation against CTRL are averaged for  
319 the monsoon season and region covering TP and Indo Gangetic Plains (15°N -35°N; 80°E -  
320 110°E) (see Table-1). The seasonal mean anomaly of aerosol forcing for Demiss simulation is  
321  $+0.37 \pm 0.26 \text{ W m}^{-2}$  at the Top Of the Atmosphere (TOA) and  $-4.74 \pm 1.42 \text{ W m}^{-2}$  at the surface.  
322 The estimated aerosol forcing anomalies for DBConly (DOConly) simulation is  $+0.31 \pm 0.25 \text{ W}$   
323  $\text{m}^{-2}$  ( $-0.51 \pm 0.32 \text{ W m}^{-2}$ ) at the TOA and  $-4.20 \pm 0.81 \text{ W m}^{-2}$  ( $-1.96 \pm 0.95 \text{ W m}^{-2}$ ) at the surface. In  
324 comparison, AR5 assessment of global mean BC RF at the TOA is  $+0.4 \text{ W m}^{-2}$  (Myhre et al.,  
325 2013). The atmospheric RF is computed from the difference between forcing at TOA and  
326 surface. It represents the energy trapped in the atmosphere due to the presence of higher amounts  
327 of carbonaceous aerosols. The resultant anomaly of atmospheric aerosol RF for Demiss is  
328  $+5.11 \pm 0.83 \text{ W m}^{-2}$ , and for DBConly (DOConly)  $+4.52 \pm 0.38 \text{ W m}^{-2}$  ( $+1.45 \pm 0.49 \text{ W m}^{-2}$ ). Table-1  
329 indicates that among the carbonaceous aerosols, the major contribution in enhancing atmospheric  
330 RF is due to BC aerosols although emission of OC higher than BC aerosols over Asia. This may  
331 be due to scattering and absorbing property of OC aerosols. From athelometer observations,  
332 Sreekanth et al., (2007) reported BC RF at the TOA  $+2.36 \text{ W m}^{-2}$  and  $-9.9 \text{ W m}^{-2}$  at the surface at  
333 Visakhapatnam (17°7'N, 83°3'E) during the monsoon season of the year 2006. These values are  
334 higher than anomalies of BC RF (DBConly-CTRL) (TOA  $+1.3 \pm 0.80 \text{ W m}^{-2}$  and surface -

335  $5.0 \pm 1.31 \text{ W m}^{-2}$ ) obtained at the grid centred at Visakhapatnam. These differences may be due to  
336 a comparison of point observations at Visakhapatnam with model output extracted over a grid  
337 ( $1.875^\circ \times 1.875^\circ$ ) centred at the same location. Also, BC aerosols are underestimated in the model  
338 (Fig.2a-c). Pan et al (2015) has shown model simulations with AEROCOM-ACCMIP-II  
339 emissions underestimate AOD over south Asia (15% to 44 %) in comparison with Multi-angle  
340 Imaging Spectro Radiometer observations.

341 The resulting short-wave plus long-wave atmospheric forcing due to doubled  
342 carbonaceous aerosols will translate to a significant atmospheric heating (Babu et al., 2002). We  
343 obtain anomalies in total Heating Rates (HR) due to carbonaceous aerosols (Demiss - CTRL).  
344 Figures 4c and 4d show longitude-pressure (averaged for  $15^\circ\text{N} - 35^\circ\text{N}$ ) and latitude-pressure  
345 (averaged for  $80^\circ\text{E} - 110^\circ\text{E}$ ), cross sections of HR anomalies during the monsoon season.  
346 Enhanced carbonaceous aerosols emissions increase HR near the surface over the Indo-Gangetic  
347 Plains, southern slopes of the Himalayas and south China. High emissions from these regions  
348 cause anomalous heating ( $0.08 \text{ K day}^{-1}$ ) in the lower troposphere (1000 hPa - 600 hPa). Positive  
349 anomalies of HR can be seen along the pathway through which carbonaceous aerosols are  
350 transported into the anticyclone. The carbonaceous aerosols have increased HR by  $\sim 0.02 \text{ K day}^{-1}$   
351 -  $0.03 \text{ K day}^{-1}$  near the tropopause in the ASM region in comparison with CTRL simulations  
352 ( $0.006 \text{ K day}^{-1} - 0.01 \text{ K day}^{-1}$ ). FigureS2 exhibits latitude-pressure cross section of HR anomalies  
353 for DBConly and DOConly simulations. It can be seen that in transport pathways, anomalies of  
354 HR for DBConly simulation are higher than DOConly although emissions of OC aerosols are  
355 higher than BC over Asia. This heating may be attributed to the high absorbing property of BC  
356 than OC. It can be seen that HR obtained from Demiss-CTRL simulations is not just arithmetic  
357 summation of HR from DBConly-CTRL and DOConly-CTRL. This may be due to nonlinear



358 dynamical changes due to heating by BC and cooling/heating effects of OC (Penner et al., 1998).  
359 Radiative heating of the tropopause region increases the vertical motion and transport into the  
360 lower stratosphere (Gettelman et al., 2004). Carbonaceous aerosol anomalies enhancement ( $>2$   
361  $\text{ng m}^{-3}$ ) in the lower stratosphere seen in Figs. 4a and 4b is due to increase in vertical motion in  
362 response to enhanced aerosol HR. This indicates that aerosols induce positive feedback in  
363 vertical transport.

#### 364 **4.2 Impact on temperature, circulation and precipitation**

365 Further, we analyze changes in temperature induced by doubled carbonaceous aerosol  
366 emissions. Figures 4e and 4f show the longitude-pressure (averaged over  $15^{\circ}\text{N} - 35^{\circ}\text{N}$ ) and  
367 latitude-pressure (averaged over  $80^{\circ}\text{E} - 110^{\circ}\text{E}$ ) cross sections of temperature anomalies. These  
368 aerosols induce significant warming in the mid-troposphere (500 hPa - 300 hPa) over the ASM  
369 region (Fig. 4e) and an anomalous warm core (warming  $\sim 1\text{K}$ ) in the mid-upper troposphere  
370 ( $\sim 400$  hPa - 300 hPa) over the TP (Fig. 4f). This warming may be due to heating by aerosol and  
371 water vapour together. The aerosol induced warming may enhance water vapour transport in the  
372 mid/upper troposphere (discussed in section 4.3) in response to dynamical changes. The  
373 enhanced water vapour would contribute additionally to this warming and provide positive  
374 feedback (Fig 8 a-b). The warming over TP in response to doubling of BC (DBConly) and OC  
375 (DOConly) aerosols individually is shown in Fig.S3. Warming due to BC aerosols is  $\sim 0.3\text{K} -$   
376  $1.2\text{K}$  over the TP while OC aerosols show cooling ( $-0.3\text{K}$ ) over central TP and warming ( $+0.6\text{K}$ )  
377 over northern TP. This indicates that BC aerosols play a major role in creating a warm core over  
378 the TP. This warm core extends to mid-high latitudes. **It is related to warming by BC aerosols**  
379 **and partially by water vapour. Figure S4 shows that BC aerosols are transported upward and**  
380 **northward from (latitudes  $40^{\circ}\text{N} - 48^{\circ}\text{N}$ ) regions of China, Mongolia, and southern Russia to the**

381 mid latitude upper troposphere which might have contributed to this warming. In addition, the  
382 negative water vapour anomalies in the same region seen in Figure 8b imply a decreased  
383 radiative cooling and this might have partially contributed towards the warming anomaly. The  
384 warm core over the TP plays an important role in enhancing the ASM circulation (Flohn 1957;  
385 Yanai et al., 1992; Meehl, 1994; Li and Yanai, 1996; Wu and Zhang, 1998) (discussed later in  
386 this section). Figure 4e shows cooling near the tropopause in the anticyclone region with a small  
387 patch of positive anomalies over the TP (80°E-100°E). During the monsoon season, cold  
388 temperatures in the UTLS persist the over warm mid-troposphere (Randel and Park 2006; Park et  
389 al., 2007). Our model simulations show that doubling of carbonaceous aerosol emissions  
390 amplifies the mid-tropospheric warming and cooling near the tropopause. The mid-upper  
391 tropospheric warming would enhance convective instability (Defouw, 1970). The strong negative  
392 anomalies in Brunt–Väisälä frequency (an indication of strong convective instability) in the mid-  
393 upper troposphere (300 hPa - 200 hPa) confirm (Fig. 5a) positive feedback between warming and  
394 convective instability in the mid-upper troposphere.

395 During Northern hemispheric summer, heating over the TP maintains a large-scale  
396 thermally driven vertical circulation (Yanai et al., 1992). The analysis of simulated vertical  
397 velocities shows that carbonaceous aerosols induce positive anomalies over the southern slope of  
398 Himalayas and Indo-Gangetic plains (Figs 5b and 5c). Thus carbonaceous aerosols amplify  
399 warming (Fig. 4e and Fig. 4f) and enhance ascending motion over these regions. Previous studies  
400 (Rajagopalan and Molnar, 2013, Vinoj et al., 2014) have reported that the warm ascending air  
401 above the TP gradually spreads southward and descends over the northern Indian Ocean. The  
402 south-westerly winds at the surface, on the other hand, complete the monsoon Hadley cell. This  
403 local circulation system releases latent heat and further maintains the Tibetan warm core. Thus

404 heating over the TP leads to increased Indian summer monsoon rainfall by enhancing the cross-  
405 equatorial circulation and concurrently strengthening both the Somali Jet (low level Jet) and the  
406 westerly winds that bring rainfall to India. Goswami et al., (1999) also reported that there is a  
407 strong correlation between monsoon Hadley circulation and precipitation. Figure 5d shows that  
408 carbonaceous aerosols strengthen the monsoon Hadley circulation, ascending motion over 10°N -  
409 20°N and descending over 0°-10°S. These aerosols reinforce low-level monsoon jet (850hPa)  
410 (seen in Fig. 5e and also Fig.5d) and outgoing long-wave radiation (Fig. 5e). Figure 5e show  
411 enhanced convection (negative anomalies in OLR) is induced by the carbonaceous aerosols over  
412 the Arabian Sea, Bay of Bengal, and a majority of the Indian subcontinent, Myanmar and East  
413 China region.

414 The carbonaceous aerosols also indirectly affect precipitation processes by altering the  
415 CCN and Cloud Droplet Number Concentration (CDNC) (Rosenfeld et al., 2002). In our model  
416 simulations, doubling of carbonaceous aerosols and related indirect effect result in enhancement  
417 of CDNC ( $8 \text{ m}^{-3}$  -  $12 \text{ m}^{-3}$ ) and cloud water ( $5 \mu\text{g m}^{-3}$  -  $20 \mu\text{g m}^{-3}$ ) in the region of strong  
418 convection (The Bay of Bengal, southern slopes of the Himalayas and South China Sea) in the  
419 lower troposphere (Fig.6a-d).

420 Figures 4-6 suggest that enhanced emissions of carbonaceous aerosols increase the HR,  
421 and amplify warm anomalies in the middle troposphere and cold anomalies near the tropopause.  
422 Aerosol induced warming elicits enhancement in vertical velocities. These aerosols induce an  
423 anomalous warming over the TP which in turn strengthens the monsoon Hadley circulation, low  
424 level monsoon jet and convection over the Indian subcontinent and East China. Previous studies  
425 (Meehl et al., 1994; Krishnamurthy and Achuthavarier, 2012) have explained the mechanism of  
426 strengthening of the monsoon Hadley circulation facilitates enhance precipitation over the Indian

427 region. Consequently, aerosol (carbonaceous) induced precipitation anomalies are positive over  
428 the Indian region ( $1 \text{ mm day}^{-1} - 4 \text{ mm day}^{-1}$ ) (Fig. 7a). Strong positive anomalies ( $2 \text{ mm day}^{-1} - 4$   
429  $\text{mm day}^{-1}$ ) are located over North India, the Bay of Bengal, Western coast of India and foothills  
430 of Himalaya. There is an enhancement in precipitation over North east China ( $0.2 \text{ mm day}^{-1} - 2$   
431  $\text{mm day}^{-1}$ ) and some parts of central and south China ( $0.2 \text{ mm day}^{-1} - 1 \text{ mm day}^{-1}$ ). We show  
432 anomalies in precipitation obtained from DBConly and DOConly with respect to CTRL in Figs.  
433 7b-c. These figures show that BC aerosols induce positive precipitation anomalies ( $\sim 1 \text{ mm day}^{-1}$   
434  $- 5 \text{ mm day}^{-1}$ ) over the Indian region by strengthening of monsoon Hadley circulation (Fig.S5a)  
435 while OC aerosols elicit negative precipitation anomalies over India ( $-1 \text{ mm day}^{-1} - -5 \text{ mm day}^{-1}$ ),  
436 north eastern China ( $0 - -1 \text{ mm day}^{-1}$ ) by producing subsidence over these regions (Fig. S5b). In  
437 agreement with the present study, aerosol-climate modeling studies by Wang et al., (2004, 2007)  
438 also show enhancement in precipitation over India due to black carbon direct RF. Increase in the  
439 Indian summer monsoon precipitation due to the loading of absorbing aerosol (BC and dust) has  
440 been reported in the past (Lau and Kim., 2006; Vinoj et al., 2014; Fadnavis et al., 2016). In the  
441 current study, simulations are performed with prescribed SSTs. In the model setup, interactive  
442 aerosols change the meteorology and feedback to aerosols variations. Other model studies using  
443 prescribed SSTs (Chung et al., 2002; Menon et al., 2002; Lau and Kim, 2006) also show an  
444 increase in precipitation over India due to black carbon aerosols. These model simulations did  
445 not take into account aerosol feedback with SSTs, unlike coupled atmosphere-ocean general  
446 circulation model. However, ocean-atmosphere coupled models often need multi-century  
447 simulations to take into account slow response of SSTs (Danabasoglu and Gent, 2009). The  
448 coupled atmosphere slab ocean model by Ganguly et al. (2012) show a mix response of  
449 precipitation distribution on climate scale. It shows a reduction in precipitation over the western

450 coast line of the Indian peninsula and an increase over north western part of Indian subcontinent.  
451 Reduction in precipitation is attributed to anthropogenic aerosols from Asia and remote  
452 locations. These differences are due to different model-set up; present study gives an impact of  
453 doubled Asian carbonaceous aerosol emissions using aerosol-atmosphere-climate model. On the  
454 other hand, Ganguly et al. (2012) show responses of all anthropogenic and biomass burning  
455 aerosols in the context of climatic change (pre-industrial and present day) accounting also the  
456 slow response of SSTs.

### 457 **4.3 Impact on water vapour and cloud ice**

458 Recently from satellite observations, Park et al., (2007) have shown that water vapour in  
459 the upper troposphere (~216 hPa) varies coherently with deep monsoon convection both  
460 temporally and spatially. Transport of high water vapour in the UTLS by the monsoon  
461 convection has been reported in the past (Gettelman et al., 2004; Dessler and Sherwood, 2004;  
462 Fu et al., 2006; Randel and Park, 2006, Braesicke et al., 2011; Ploeger et al., 2013). We analyze  
463 the difference in water vapour anomalies (Demiss - CTRL) to understand the impact of doubled  
464 Asian carbonaceous aerosol emissions on the transport of water vapour in the UTLS. Figures 8a  
465 and 8b show an increase in water vapour in the upper troposphere and lower stratosphere 3% -  
466 15% (~0.1 ppmv - 20 ppmv). Water vapour anomalies 10 % - 15% (~8 ppmv - 20 ppmv) are  
467 seen near 200 hPa and 1 % - 5% (~0.1 ppmv - 0.8 ppmv) near the tropopause. Fadnavis et al.  
468 (2013) reported an increase in water vapour (~ 0.1 ppmv - 10 ppmv) in the UTLS in response to  
469 the increasing aerosols which are in agreement with the current study. In the past, Gettleman et  
470 al. (2004), Fu et al. (2006), Fadnavis et al., (2013), Garny and Randel (2016) also reported  
471 transport of water vapour above the tropopause into the lower stratosphere during the monsoon  
472 season. Enhanced aerosol emissions increase water vapour transport into the lower stratosphere

473 by enhancing HRs, mid/upper tropospheric warming, and vertical velocities. These elevated  
474 levels of water vapour will provide positive feedback by intensifying the HRs.

475 In addition to thermal and dynamical impact, aerosols in the UTLS also largely influence  
476 the formation and microphysical properties of cirrus clouds. Cirrus clouds have a great impact on  
477 radiation and intensity of the large-scale tropical circulation (Randall et al., 1989; Ramaswamy  
478 and Ramanathan, 1989; Liu et al., 2003). Figures 8c –8f show longitude-pressure and latitude-  
479 pressure cross sections of anomalies of cloud ice and Ice Crystal Number Concentration (ICNC).  
480 These figures show enhancement of anomalies of cloud ice (by  $0.4 \mu\text{g m}^{-3} - 2 \mu\text{g m}^{-3}$ ) and ICNC  
481 (by  $0.001 \text{ m}^{-3} - 0.01 \text{ m}^{-3}$ ) occurrence in the upper troposphere (350 hPa - 100 hPa). Maximum  
482 increase (cloud ice by  $2 \mu\text{g m}^{-3}$ , ICNC by  $0.01 \text{ m}^{-3}$ ), is seen in the  $80^\circ\text{E} - 90^\circ\text{E}$ ,  $20^\circ\text{N} - 30^\circ\text{N}$  where  
483 stronger upwelling motion prevails (Figs. 8e and 8f). A fraction of positive anomalies of ICNC is  
484 seen near the tropopause indicating entrainment into the lower stratosphere. Positive anomalies  
485 in cloud ice and ICNC (in the upper troposphere) are due to enhancement in ASM deep  
486 convection (increase in heating rates, mid/upper tropospheric temperature, vertical velocity, and  
487 monsoon Hadley circulation) induced by the doubling of carbonaceous aerosols emissions.

488

## 489 **5. Summary and conclusions**

490 In this paper, we investigated impacts of enhanced Asian ( $65^\circ\text{E} - 155^\circ\text{E}$ ;  $10^\circ\text{S} - 50^\circ\text{N}$ )  
491 carbonaceous aerosols on the UTLS, monsoon circulation and precipitation over India and China  
492 using a state of the art aerosol-climate model. We performed sensitivity experiments for doubling  
493 of carbonaceous aerosol emission over the Asian region.

494 To validate the model simulations, we compare simulated BC vertical profile with  
495 observations from aircraft measurements at Guwahati ( $26^\circ 11'\text{N}$ ,  $91^\circ 44'\text{E}$ ) India during August-

496 September 2009 and athelometer launched on Balloonsonde at Hyderabad (78°E, 17°N) on 17  
497 March 2010 (pre-monsoon season); seasonal mean of simulated cloud ice content with  
498 climatology of combined measurements from CloudSat and CALIPSO (2007 - 2010); and  
499 simulated precipitation with climatology of TRMM observations (1997 - 2016).The aircraft  
500 measurements show reasonable agreement with BC concentrations obtained from doubling of  
501 carbonaceous aerosol simulation (Demiss) in the lower troposphere. In the troposphere, the  
502 difference between aircraft measurements and simulated BC vary with altitude. Balloonsonde  
503 measurements at Hyderabad show large differences with Demiss simulations in the troposphere.  
504 The spatial patterns of the simulated season mean (June - September) precipitation are  
505 comparable with climatology of TRMM precipitation (1997- 2016) and cloud ice with combined  
506 measurements from CloudSat and CALIOP (2007 - 2010) respectively. Simulated cloud ice is  
507 underestimated  $2 \text{ mg kg}^{-1}$  -  $7 \text{ mg kg}^{-1}$  in the UTLS (60°E - 120°E; 15°N - 40°N) during the  
508 summer monsoon season.

509 Our model simulations show that monsoon convection over the Bay of Bengal, the South  
510 China Sea and Southern flanks of the Himalayas transport Asian carbonaceous aerosol into the  
511 UTLS. A persistent maximum of carbonaceous aerosols is seen within the anticyclone during the  
512 ASM season, and a fraction of these aerosols enter the lower stratosphere. Doubling emissions of  
513 carbonaceous aerosol over the Asian region leads to their enhancement (by  $4 \text{ ng m}^{-3}$ -  $6 \text{ ng m}^{-3}$ ) in  
514 the UTLS. They alter aerosol RF at the surface by  $-4.74 \pm 1.42 \text{ W m}^{-2}$ ; at the TOA by  $+0.37 \pm 0.26$   
515  $\text{W m}^{-2}$  and in the atmosphere by  $+5.11 \pm 0.32 \text{ W m}^{-2}$  over TP and Indo Gangetic Plains. Positive  
516 anomalies of heating rates are seen along the pathway through which aerosols are transported  
517 into the anticyclone. These carbonaceous aerosols increase heating rates in the anticyclone ( $\sim 100$   
518 hPa) by  $0.02 \text{ K day}^{-1}$  -  $0.03 \text{ K day}^{-1}$ . They induce significant warming (temperature increases by

519 1 K) in the mid/upper troposphere over the ASM region. An anomalous in-atmospheric warming  
520 enhances vertical velocities and thereby cloud ice ( $2 \text{ mg m}^{-3}$ ), ICNC ( $0.01 \text{ m}^{-3}$ ). A significant  
521 increase in water vapour transport in the upper troposphere 10% -15% (0.5 ppmv -10 ppmv) and  
522 1% - 5 % (0.1 ppmv - 0.5 ppmv) near the tropopause is apparently related to the mid/upper  
523 tropospheric warming. Doubling of carbonaceous aerosols emissions enhance warming over the  
524 TP ( $\sim 1\text{K}$ ) and cold anomalies near the tropopause. The warming over TP may be partially due to  
525 heating by water vapour creating a positive feedback. The enhanced carbonaceous aerosols  
526 strengthen the monsoon Hadley circulation by intensifying warming over TP. They strengthen  
527 the low level monsoon jet, convection and elicit precipitation enhancement over India ( $1 \text{ mm}$   
528  $\text{day}^{-1}$  -  $4 \text{ mm day}^{-1}$ ) and eastern China ( $0.2 \text{ mm day}^{-1}$  -  $2 \text{ mm day}^{-1}$ ). In agreement with the present  
529 study, aerosol-climate modeling studies by Wang et al., (2004, 2007) also show enhancement in  
530 Indian summer monsoon precipitation due to black carbon direct RF.

531 The experiments with doubling of BC only (DBConly) and OC only (DOConly) aerosols  
532 indicate that the HRs due to BC is higher that of OC aerosols along the transport path ways (the  
533 Bay of Bengal and southern slope of the Himalayas). BC aerosol induces anomalous warming  
534 over the TP and enhances positive precipitation anomalies ( $\sim 1 \text{ mm day}^{-1}$  -  $5 \text{ mm day}^{-1}$ ) over the  
535 Indian region by strengthening of monsoon Hadley circulation. While, OC aerosol produces  
536 cooling over central TP and elicits negative precipitation anomalies over India ( $-1 \text{ mm day}^{-1}$  -  $-5$   
537  $\text{mm day}^{-1}$ ) and north eastern China ( $0$  -  $-1 \text{ mm day}^{-1}$ ) by producing subsidence over these  
538 regions.

539 In the current study, simulations are performed with enhanced Asian carbonaceous aerosols  
540 and prescribed SSTs where interactive aerosols change the meteorology and feedback to aerosols  
541 variations. Other modeling studies using prescribed SSTs and increase in global BC emissions



542 also show an increase in precipitation over India (Chung et al., 2002; Menon et al., 2002; Lau et  
543 al., 2006). Observational evidence also shows that heavy loading of absorbing aerosols (BC and  
544 Dust) over the Indian subcontinent facilitate the enhancement of monsoon rainfall over India  
545 (Lau and Kim, 2006; Vinoj et al., 2014).

546 We note that a realistic future emission scenario also includes the increasing emissions of  
547 sulfate aerosols and the response of climate and circulation to increasing CO<sub>2</sub> concentrations,  
548 which might interplay with the presented results and lead to different dynamical and climatic  
549 responses. Moreover, in future, we propose to re-evaluate the studies by using the regional model  
550 with a better resolution of the complex orography over Himalayas/TP, etc. Notwithstanding this,  
551 the work provides valuable insight into the influence of growing Asian carbonaceous aerosols  
552 emissions on the UTLS, connecting monsoon processes and precipitation in the Asian summer  
553 monsoon region.

554 *Acknowledgement:* Authors acknowledges with gratitude the High Power Computing  
555 Centre (HPC) in IITM, Pune, India, for providing computer resources. **Authors are thankful to**  
556 **anonymous reviewers and Co-Editor for valuable suggestions.**

557 |

558 **References:**

- 559
- 562 Ackerman, A. S., Toon, O.B., Stevens, D.E., Heymsfield, A.J., Ramanathan,V., Welton,E,J.:
- 563 Reduction of tropical cloudiness by soot, *Science*, 288,1042-1047, doi:
- 564 10.1126/science.288.5468.1042,2000.
- 567 Babu, S. S., S. K. Satheesh, and K. K. Moorthy.: Aerosol radiative forcing due to enhanced black
- 568 carbon at an urban site in India, *Geophys. Res. Lett.*, 29, 1880,
- 569 doi:10.1029/2002GL015826, 2002.
- 570 Babu, S. S., K. K. Moorthy, R. K. Manchanda, P. R. Sinha, S. K. Satheesh, D. P. Vajja, S.
- 571 Srinivasan, V. H. A. Kumar.: Free tropospheric black carbon aerosol measurements
- 572 using high altitude balloon: Do BC layers build “their own homes” up in the
- 573 atmosphere?, *Geophys. Res. Lett.*, 38, L08803, doi:10.1029/2011GL046654, 2011.
- 576 Badarinath, K. V. S. and Latha, M. K., Direct radiative forcing from black carbon aerosols over
- 577 urban environment, *Advances in Space Research*, Volume 37, Issue 12, p. 2183-2188,
- 578 10.1016/j.asr.2005.10.034, 2006.
- 579 Baron, R.E., Montgomery, W.D., Tuladhar, S.D.,. An Analysis of Black Carbon Mitigation as a
- 580 Response to Climate Change, [http://fixtheclimate.com/component-1/the-result-](http://fixtheclimate.com/component-1/the-result-prioritization/)
- 581 [prioritization/](http://fixtheclimate.com/component-1/the-result-prioritization/), accessed in February 2010, 2009.
- 582 Bond, T. C., Streets, D. G., Yarber, K. F., Nelson, S. M., Woo, J.-H., and Klimont, Z.: A
- 583 technology-based global inventory of black and organic carbon emissions from
- 584 combustion, *J. Geophys. Res.*, 109, D14203, doi:10.1029/2003JD003697, 2004.
- 587 Bond, T.C., S. J. Doherty, D. W. Fahey, P. M. Forster,T. Berntsen, B. J. DeAngelo, M. G.
- 588 Flanner, S. Ghan, B. Kärcher, D. Koch, S. Kinne, Y. Kondo, P. K. Quinn, M. C. Sarofim,
- 589 M. G. Schultz, M. Schulz, C. Venkataraman, H. Zhang, S. Zhang, N. Bellouin, S. K.
- 590 Guttikunda, P. K. Hopke, M. Z. Jacobson, J. W. Kaiser, Z. Klimont, U. Lohmann, J. P.
- 591 Schwarz, D. Shindell, T. Storelvmo, S. G. Warren, and C. S. Zender.: Bounding the role
- 592 of black carbon in the climate system: A scientific assessment, *Journal Of Geophysical*
- 593 *Research: Atmospheres*, Vol. 118, 5380–5552, doi:10.1002/jgrd.50171, 2013.
- 594 Braesicke, P., O. J. Smith, P. Telford, and J. A. Pyle.:Ozone concentration changes in the Asian
- 595 summer monsoon anticyclone and lower stratospheric water vapour: An idealised model
- 596 study, *Geophys. Res. Lett.*, 38, L03810, doi:10.1029/2010GL046228,2011.

597 Butt, E. W. Rap A., Schmidt A., Scott C. E., Pringle K. J., Reddington1 C. L., Richards N. A. D.,  
598 Woodhouse M. T., Ramirez-Villegas J., Yang H., Vakkari V., Stone E. A., Rupakheti M.,  
599 Praveen P. S., van Zyl P. G., Beukes J. P., Josipovic M., Mitchell E. J. S., Sallu S. M.,  
600 Forster P. M., and Spracklen D. V.: The impact of residential combustion emissions on  
601 atmospheric aerosol, human health, and climate, *Atmos. Chem. Phys.*, 16, 873–905,  
602 doi:10.5194/acp-16-873-2016, 2016.

605 Carmichael, G. H., Bhupesh Adhikary, Sarika Kulkarni, Alessio D’Allura, Youhua Tang, David  
606 Streets, Qiang Zhang, TamI C. Bond, Veerabhadran Ramanathan, Aditsuda Jamroensan,  
607 and Pallavi Marrapu, *Asian Aerosols: Current and Year 2030 Distributions and*  
608 *Implications to Human Health and Regional Climate Change*, *Environ. Sci. Technol.*, 43,  
609 5811–5817, doi:10.1021/es8036803, 2009.

610 Cheng, T., Y. Peng, J. Feichter, and I. Tegen.: An Improvement on the dust emission scheme in  
611 the global aerosol-climate model ECHAM5-HAM, *Atmos. Chem. Phys.*, 8, 1105-1117,  
612 doi:10.5194/acp-8-1105-2008, 2008.

613 Chin, M., Diehl, T., Dubovik, O., Eck, T. F., Holben, B. N., Sinyuk, A., and Streets, D. G.: Light  
614 absorption by pollution, dust, and biomass burning aerosols: a global model study and  
615 evaluation with AERONET measurements, *Ann. Geophys.*, 27, 3439–3464,  
616 doi:10.5194/angeo-27-3439-2009, 2009.

617 Chung, S. H., and J. H. Seinfeld.: Global distribution and climate forcing of carbonaceous  
618 aerosols, *J. Geophys. Res.*, 107(D19), 4407, doi:10.1029/2001JD001397, 2002.

619 Danabasoglu, G., and P. Gent Equilibrium climate sensitivity: Is it accurate to use a slab ocean  
620 model?, *J. Clim.*, 22, 2494–2499, doi:10.1175/2008JCLI2596.1, 2009.

621 Defouw, R.J., *Thermal-Convective Instability*, *Astrophysical Journal*, 160, 659-669, 1970.

622 Deng, M., G. G. Mace, Z. Wang, and H. Okamoto.: Tropical Composition, Cloud and Climate  
623 Coupling Experiment validation for cirrus cloud profiling retrieval using CloudSat radar and  
624 CALIPSO lidar, *J. Geophys. Res.*, 115, D00J15, doi:10.1029/2009JD013104, 2010.

625 Deng, M., G. G. Mace, Z. Wang, and Lawson, R. P.: Evaluation of Several A-Train Ice Cloud  
626 Retrieval Products with In Situ Measurements Collected during the SPARTICUS Campaign,  
627 *Journal Of Applied Meteorology And Climatology*, 52, 1014-1030, doi: 10.1175/JAMC-D-  
628 12-054.1, 2013.

629 Dentener, F., Kinne,S., Bond,T., Boucher,O., Cofala, J., Generoso, S., Ginoux, P., Gong,S.,  
630 Hoelzemann, J., Ito,A., Marelli,L., Penner, J., Putaud, J.P., Textor, C., Schulz, M.,  
631 G.V.D., Werf, Wilson J.: Emissions Of primary aerosol and precursor gases in the years  
632 2000 and 1750 prescribed data -sets for AeroCom, *Atmos. Chem. Phys.*, 6, 4321-4344,  
633 doi:10.5194/acp-6-4321-2006,2006.

634 Dessler, A. E., and S. C. Sherwood.: Effect of convection on the summertime extratropical lower  
635 stratosphere, *J. Geophys. Res.*, 109, D23301, doi:10.1029/2004JD005209, 2004.

636 Fadnavis, S., Semeniuk, K., Pozzoli, L., Schultz, M. G., Ghude, S. D., Das, S., and Kakatkar,  
637 R.: Transport of aerosols into the UTLS and their impact on the Asian monsoon region  
638 as seen in a global model simulation, *Atmos. Chem. Phys.*, 13, 8771–8786,  
639 doi:10.5194/acp-13-8771-2013, 2013.

640 Fadnavis, S., Schultz, M. G., Semeniuk, K., Mahajan, A. S., Pozzoli, L., Sonbawne, S., Ghude,  
641 S. D., Kiefer, M., and Eckert, E.: Trends in peroxyacetyl nitrate (PAN) in the upper  
642 troposphere and lower stratosphere over southern Asia during the summer monsoon  
643 season: regional impacts, *Atmos. Chem. Phys.*, 14, 12725–12743, doi:10.5194/acp-14-  
644 12725-2014, 2014.

645 Fadnavis, S., Semeniuk, K., Schultz, M. G., Kiefer, M., Mahajan, A., Pozzoli, L., and  
646 Sonbawane, S.: Transport pathways of peroxyacetyl nitrate in the upper troposphere and  
647 lower stratosphere from different monsoon systems during the summer monsoon season.  
648 *Atmos. Chem. Phys.*, 15, 11477-11499, doi:10.5194/acp-15-11477-2015, 2015.

649 Fadnavis, S.; Roy, Chaitri; Sabin, T. P.; Ayantika, D. C.; Ashok, K.: Potential modulations of  
650 pre-monsoon aerosols during El Niño: impact on Indian summer monsoon, *Clim.Dyn.*,1-  
651 12,doi: 10.1007/s00382-016-3451-6, 2016.

652 Flohn, H.: Large-scale aspects of the summer monsoon in South and East Asia, *J. Meteor. Soc.*  
653 Japan, 75, 180–186, doi: 551.553.21:551.589.5, 1957.

655 Fu, R., Hu, Y., Wright, J. S., Jiang, J. H., Dickinson, R. E., Chen, M., Filipiak, M., Read,W.  
656 G.,Waters, J.W., and Wu, D. L.: Short circuit of water vapour and polluted air to the  
657 global stratosphere by convective transport over the Tibetan Plateau, *P. Natl. Acad. Sci.*  
658 USA, 103, 5664–5669, doi: 10.1073/pnas.0601584103, 2006.

659 Ganguly, D., P. J. Rasch, H. Wang, and J.-H. Yoon, Climate response of the South Asian  
660 monsoon system to anthropogenic aerosols, *J. Geophys. Res.*, 117, D13209,  
661 doi:10.1029/2012JD017508, 2012.

662 Garny, H. and Randel, W. J.: Transport pathways from the Asian monsoon anticyclone to the  
663 stratosphere, *Atmos. Chem. Phys.*, 16, 2703–2718, doi:10.5194/acp-16-2703-2016,2016.

664 Gautam R., Hsu N. C., Tsay S. C., Lau K. M., Holben B., Bell S., Smirnov A., Li C., Hansell R.,  
665 Ji Q., Payra S., Aryal D., Kayastha R., and Kim K. M.: Accumulation of aerosols over the  
666 Indo-Gangetic plains and southern slopes of the Himalayas: distribution, properties and  
667 radiative effects during the 2009 pre-monsoon season, *Atmos. Chem. Phys.*, 11, 12841–  
668 12863, doi:10.5194/acp-11-12841-2011, 2011.

669 Gettelman, A., Forster, P., Fujiwara, M., Fu, Q., Vomel, H., Gohar, L. K., Johanson, C., and  
670 Ammerman, M.: Radiation balance of the tropical tropopause layer, *J. Geophys. Res.*,  
671 109, D07103, doi:10.1029/2003JD004190, 2004.

672 Goswami, B. N., V. Krishnamurthy, and H. Annamalai, 1999: A broad scale circulation index for  
673 the interannual variability of the Indian summer monsoon. *Q. J. R. Meteorol. Soc.*, 125,  
674 pp. 611-633, doi: 10.1002/qj.49712555412, 1999.

675 Govardhan, G., Satheesh, S.K., Nanjundiah,R., Krishna Moorthy, K., and Babu, S. S.: Possible  
676 climatic implications of high altitude emissions of black carbon, *Atmos. Chem. Phys.*  
677 *Discuss.*, doi:10.5194/acp-2017-96, 2017.

678 Guelle, W., Schulz, M., Balkanski,Y., Dentener, F.: Influence of the source formulation on  
679 modeling the atmospheric global distribution of sea salt aerosol, *J. Geophys. Res.*, 106,  
680 27509-27524, doi:10.1029/2001JD900249,2001.

681 Guenther, A., Hewitt, C. N., Erickson, D., Fall, R., Geron, C., Graedel, T., Harley, P., Klinger,  
682 L., Lerda, M., Mckay, W. A., Pierce, T., Scholes, B., Steinbrecher, R., Tallamraju, R.,  
683 Taylor, J., and Zimmerman, P. A.: Global-Model of Natural Volatile Organic-Compound  
684 Emissions, *J. Geophys. Res.- Atmos.*, 100, 8873–8892, doi: 10.1029/94JD02950, 1995.

685 Guo L., Highwood E. J., Shaffrey L. C., and Turner A. G.: The effect of regional changes in  
686 anthropogenic aerosols on rainfall of the East Asian Summer Monsoon, *Atmos. Chem.*  
687 *Phys.*, 13, 1521-1534, doi:10.5194/acp-13-1521-2013, 2013.

688 Guo, L., Turner, A.G. and Highwood, E. J.: Impacts of 20th century aerosol emissions on the  
689 South Asian monsoon in the CMIP5 models, *Atmos. Chem. Phys.*, 15, 6367–6378,  
690 doi:10.5194/acp-15-6367-2015, 2015.

695 Haywood, J. M., Shine, K.P.: Multi-spectral calculations of the radiative forcing of tropospheric  
696 sulphate and soot aerosols using a column model, *Q. J. R. Meteorol. Soc.*, 123, 1907-  
697 1930, doi:10.1002/qj.49712354307, 1997.

698 He, Q. S., Li, C. C., Ma, J. Z., Wang, H. Q., Yan, X. L., Lu, J., Liang, Z. R., and Qi, G. M.:  
699 Lidar-observed enhancement of aerosols in the upper troposphere and lower stratosphere  
700 over the Tibetan Plateau induced by the Nabro volcano eruption, *Atmos. Chem. Phys.*,  
701 14, 11687-11696, doi:10.5194/acp-14-11687-2014, 2014.

708 Hirose, M., and K. Nakamura, Spatial and diurnal variation of precipitation systems over Asia  
709 observed by the TRMM Precipitation Radar, *J. Geophys. Res.*, 110, D05106,  
710 doi:10.1029/2004JD004815, 2005.

711 Hodnebrog, O., Myhre, G., Samset, B.H. : How shorter black carbon lifetime alters its climate  
712 effect, *Nature Communications*, 5, doi:10.1038/ncomms6065, 2014.

713 Huffman, G.J., R.F. Adler, D.T. Bolvin, G. Gu, E.J. Nelkin, K.P. Bowman, Y. Hong, E.F.  
714 Stocker, D.B. Wolff.: The TRMM Multi-satellite Precipitation Analysis: Quasi-Global,  
715 Multi-Year, Combined-Sensor Precipitation Estimates at Fine Scale. *J.*  
716 *Hydrometeor.*, 8(1) ,38-55, doi: <http://dx.doi.org/10.1175/jhm560.1>, 2007.

717 Jacobson, M. C., Hansson, H.-C., Noone, K. J., and Charlson, R. J.: Organic atmospheric  
718 aerosols: Review and state of the science, *Rev. Geophys.*, 38, 267–294,  
719 doi: 10.1029/1998RG000045, 2000.

720 Kloster, S., Dentener, F., Feichter, J., Raes, F., Lohmann, U., Roeckner, E., Burns, I.F.: A GCM  
721 study of future climate response to aerosol pollution reductions, *Clim. Dyn.*,  
722 doi:10.1007/s00382-009-0573-0, 2009.

723 Kopp, R. E., Mauzeralla D. L.: Assessing the climatic benefits of black carbon mitigation,  
724 *PNAS*, 107, 26, 11703-11708, doi: 10.1073/pnas.0909605107, 2010.

725 Krishnamurthy V, Achuthavarier D.: Intraseasonal oscillations of the monsoon circulation over  
726 South Asia. *Clim. Dyn*, 38(11):2335–2353, doi: 10.1007/s00382-011-1153-7, 2012.

727 Kumar, R., Naja, M., Satheesh, S.K., Ojha, N., Joshi, H., Sarangi, T., Pant, P., Dumka, U.C.,  
728 Hegde, P., Venkataramani, S.: Influences of the springtime northern Indian biomass

729 burning over the central Himalayas, *J. Geophys. Res.*, 116, D19302,  
730 doi:10.1029/2010JD015509, 2011.

731 Kummerow, C., Barnes, W., Kozu, T., Shiue, J. and Simpson, J.: The Tropical Rainfall  
732 Measuring Mission (TRMM) sensor package. *J. Atmos. Oceanic Technol.*, 15, 809–816,  
733 doi: [http://dx.doi.org/10.1175/1520-0426\(1998\)015<0809:TTRMMT>2.0.CO;2](http://dx.doi.org/10.1175/1520-0426(1998)015<0809:TTRMMT>2.0.CO;2), 1998.

734 Kunze M., Braesicke P., Langematz U., Stiller G., Bekki S, Brühl C., Chipperfield M., Dameris  
735 M., Garcia R, and Giorgetta M.: Influences of the Indian Summer Monsoon on Water  
736 Vapor and Ozone Concentrations in the UTLS as Simulated by Chemistry–Climate  
737 Models, 23, 3525-3544, doi: 10.1175/2010JCLI3280, 2010.

738 Lamarque, J.F., Bond, T.C., Eyring, V., Granier, C., Heil, A., Klimont, A., Lee, D., Liousse, D.,  
739 Mieville, A., Owen, B., Schultz, M.G., Shindell, D., Smith, S.J., Stehfest, E., Van  
740 Aardenne, J., Cooper, O.R., Kainuma, M., Mahowald, N., McConnell, J.R., Naik, V.,  
741 Riahi, K., van Vuuren, D.P. : Historical (1850–2000) gridded anthropogenic and biomass  
742 burning emissions of reactive gases and aerosols: methodology and application, *Atmos.*  
743 *Chem. Phys.*, 10, 7017- 7039, doi:10.5194/acp-10-7017-2010, 2010.

744 Lau, K. M., Kim, K. M.: Observational relationships between aerosol and Asian monsoon  
745 rainfall, and circulation, *Geophys. Res. Lett.*, 33, L21810, doi:10.1029/2006GL027546,  
746 2006.

747 Lelieveld, J., Crutzen, P. J., Ramanathan, V., Andreae, M. O., Brenninkmeijer, C. A. M.,  
748 Campos, T., Cass, G. R., Dickerson, R. R., Fischer, H., de Gouw, J. A., Hansel, A.,  
749 Jefferson, A., Kley, D., de Laat, A. T. J., Lal, S., Lawrence, M. G., Lobert, J. M., Mayol-  
750 Bracero, O. L., Mitra, A. P., Novakov, T., Oltmans, S. J., Prather, K. A., Reiner, T.,  
751 Rodhe, H., Scheeren, H. A., Sikka, D., and Williams, J.: The Indian Ocean Experiment:  
752 Widespread Air Pollution from South and Southeast Asia, *Science*, 291, 1031– 1036,,  
753 doi: 10.1126/science.1057103, 2001.

754 Li, C. and Yanai M.: The onset and interannual variability of the Asian summer monsoon in  
755 relation to land–sea thermal contrast, *J. Clim.* 9: 358–375, doi:  
756 [http://dx.doi.org/10.1175/1520-0442\(1996\)009,0358:TOAIVO>2.0.CO;2](http://dx.doi.org/10.1175/1520-0442(1996)009,0358:TOAIVO>2.0.CO;2), 1996.

757 Li, Q., Jiang, J. H., Wu, D. L., Read, W. G., Livesey, N. J., Waters, J.W., Zhang, Y., Wang, B.,  
758 Filipiak, M. J., Davis, C. P., Turquety, S., Wu, S., Park R. J., Yantosca R. M., and Jacob  
759 D. J.: Convective outflow of South Asian pollution: A global CTM simulation compared

760 with EOS MLS observations, *Geophys. Res. Lett.*, 32, L14826,  
761 doi:10.1029/2005GL022762, 2005.

762 Li, J.-L. F., Waliser, D.E., Chen, W.T., Guan, B., Kubar, T., Stephens, G., Ma, H.Y., Deng, M.,  
763 Donner, L., SEman, C., Horowitz, L.: An observationally based evaluation of cloud ice  
764 water in CMIP3 and CMIP5 GCMs and contemporary reanalyses using contemporary  
765 satellite data, *J. Geophys. Res.*, 117, D16105, doi:10.1029/2012JD017640, 2012.

766 Li, J.-L. F., Waliser, D. E., Stephens, G., Lee, S., L'Ecuyer, T., Kato, S., Loeb, N. and Ma, H.  
767 Y.: Characterizing and understanding radiation budget biases in CMIP3/CMIP5 GCMs,  
768 contemporary GCM, and reanalysis. *J. Geophys. Res.*, 118, 8166–8184,  
769 doi:10.1002/jgrd.50378, 2013.

770 Lin N. H., Tsay, Si-C., Maring, H.B., Yen, M.Ch., Sheu, G.R., Wang, S.H., Chi, K.H., Chuang,  
771 M.T., Chang-Feng Ou-Yang , Joshua S. Fu, Jeffrey S. Reid, Chung-Te Lee, Lin-Chi  
772 Wang, Jia-Lin Wang , Christina N. Hsu , Andrew M. Sayer, Brent N. Holben, Yu-Chi  
773 Chu, Xuan Anh Nguyen, Khajornsak Sopajaree , Shui-Jen Chen, Man-Ting Cheng, Ben-  
774 Jei Tsuang, Chuen-Jinn Tsai, Chi-Ming Peng, Russell C. Schnell, Tom Conway, Chang-  
775 Tang Chang , Kuen-Song Lin, Ying I. Tsai, Wen-Jhy Lee, Shuenn-Chin Chang, Jyh-Jian  
776 Liu, Wei-Li Chiang, Shih-Jen Huang, Tang-Huang Lin, Gin-Rong Liu.: An overview of  
777 regional experiments on biomass burning aerosols and related pollutants in Southeast  
778 Asia: From BASE-ASIA and the Dongsha Experiment to 7-SEAS, *Atmos. Environ.*, 78,  
779 1-19, <http://dx.doi.org/10.1016/j.atmosenv.2013.04.066>, 2013.

780 Lin C-Y, Zhao C., Liu X., Lin N-H ., Chen W-N.: Modelling of long-range transport of southeast  
781 Asia biomass-burning aerosols to Taiwan and their radiative forcings over EAST  
782 ASIA, *Tellus B* 2014, 66, 23733, <http://dx.doi.org/10.3402/tellusb.v66.23733>, 2014.

783 Liu, H.-L., Wang, P.K., Schlesinger, R.E.: A numerical study of cirrus clouds. Part II: Effects of  
784 Ambient Temperature, Stability, Radiation, Ice Microphysics, and Microdynamics on  
785 Cirrus Evolution. *J. Atmos. Sci.* 60, 1097–1119, doi: [http://dx.doi.org/10.1175/1520-0469\(2003\)060<1097:ansocc>2.0.co;2](http://dx.doi.org/10.1175/1520-0469(2003)060<1097:ansocc>2.0.co;2), 2003.

787 Lohmann U., Ferrachat, S.: Impact of parametric uncertainties on the present-day climate and on  
788 the anthropogenic aerosol effect, *Atmos. Chem. Phys.*, 10, 11373-11383,  
789 doi:10.5194/acp-10-11373-2010, 2010.



790 Lu, Z., Zhang, Q., Streets, D. G.: Sulfur dioxide and primary carbonaceous aerosol emissions in  
791 China and India, 1996–2010, *Atmos. Chem. Phys.*, 11, 9839–9864, doi:10.5194/acp-11-  
792 9839-2011, 2011.

793 Manoj M. G., Devara, P.C.S., Safai, P.D., Goswami, B.N.: Absorbing aerosols facilitate  
794 transition of Indian monsoon breaks to active spells, *Clim. Dyn.*, 37:2181–2198, doi:  
795 10.1007/s00382-010-0971-3,2011.

796 Meehl, G. A.: Coupled land-ocean-atmosphere processes and South Asian monsoon variability,  
797 *Science*, 266, 263–267, doi: 10.1126/science.266.5183.263, 1994.

798 Meehl G A, Arblaster J.M., Collins, W.D.: Effects of black carbon aerosols on the Indian  
799 monsoon, *J. Climate*, 21, 2869–2882, doi: <http://dx.doi.org/10.1175/2007JCLI1777.1>,  
800 2008.

801 Menon, S., Hansen, J., Nazarenko, L., and Luo, Y.: Climate Effects of Black Carbon Aerosols in  
802 China and India, *Science*, 297, 2250–2253, doi: 10.1126/science.1075159, 2002.

803 Mieville, A., C. Granier, C. Lioussé, B. Guillaume, F. Mouillot, J.F. Lamarque, J.M. Gregoire,  
804 and G. Petron.: Emissions of gases and particles from biomass burning using satellite  
805 data and an historical reconstruction, *Atmos. Environ.*, 44, 1469–1477,  
806 doi:10.1016/j.atmosenv.2010.01.011,2010.

807 Myhre, G., Shindell, D., Bréon, F. M., Collins, W., Fuglestedt, J., Huang, J., Koch, D.,  
808 Lamarque, J.-F., Lee, D., Mendoza, B., Nakajima, T., Robock, A., Stephens, G. ,  
809 Takemura T. and Zhang, H., Anthropogenic and Natural Radiative Forcing. In: *Climate*  
810 *Change 2013: The Physical Science Basis. Contribution of Working Group I to the Fifth*  
811 *Assessment Report of the Intergovernmental Panel on Climate Change* [Stocker, T.F., D.  
812 Qin, G.-K. Plattner, M. Tignor, S.K. Allen, J. Boschung, A. Nauels, Y. Xia, V. Bex and  
813 P.M. Midgley (eds.)]. Cambridge University Press, Cambridge, United Kingdom and  
814 New York, NY, USA., 2013.

815 Neubauer D., Lohmann U. and Hoose C. and Frontoso, M. G.: Impact of the representation of  
816 marine stratocumulus clouds on the anthropogenic aerosol effect *Atmos. Chem. Phys.*,  
817 14, 11997–12022, doi:10.5194/acp-14-11997-2014, 2014.

818 Pan X., Chin M., Gautam R., Bian H., Kim D., Colarco P. R., Diehl T. L., Takemura T., Pozzoli  
819 L., Tsigaridis K., Bauer S., and Bellouin N., A multi-model evaluation of aerosols over

820 South Asia: common problems and possible causes, *Atmos. Chem. Phys.*, 15, 5903–5928,  
821 doi:10.5194/acp-15-5903-2015, 2015.

822 Park, M., Randel, W.J., Gettelman, A., Massie, S.T., Jiang, J.H.: Transport above the Asian  
823 summer monsoon anticyclone inferred from Aura Microwave Limb Sounder tracers, *J.*  
824 *Geophys. Res.*, 112, D16309, doi:10.1029/2006JD008294, 2007.

825 Park, M., Randel, W.J., Emmons, L.K., Bernath, P.F., Walker, K.A., Boone, C.D.: Chemical  
826 isolation in the Asian monsoon anticyclone observed in Atmospheric Chemistry  
827 Experiment (ACE-FTS) data, *Atmos. Chem. Phys.*, doi:10.5194/acp-8-757-2008, 2008.

828 Park, M., Randel, W. J., Emmons, L. K., Livesey, N. J.: Transport pathways of carbon monoxide  
829 in the Asian summer monsoon diagnosed from Model of Ozone and Related Tracers  
830 (MOZART), *J. Geophys. Res.*, 114, D08303, doi:10.1029/2008JD010621, 2009.

831 Penner, J. E., Chuang, C.C., Grant, K.: Climate forcing by carbonaceous and sulfate aerosols,  
832 *Clim. Dyn.*, 14, 839 -851, doi:10.1007/s003820050259, 1998.

833 Ploeger, F., Fueglistaler, S., Grooß, J.-U., Günther, G., Konopka, P., Liu, Y. S., Müller, R.,  
834 Ravegnani, F., Schiller, C., Ulanovski, A., and Riese, M.: Insight from ozone and water  
835 vapour on transport in the tropical tropopause layer (TTL), *Atmos. Chem. Phys.*, 11, 407-  
836 419, doi:10.5194/acp-11- 407-2011, 2011.

837 Ploeger F., Konopka P., Müller R., Fueglistaler S., Schmidt T., Manners J., Grooss J.-U.,  
838 Günther G., de Forster P.M., and Riese M., Horizontal transport affecting trace gas  
839 seasonality in the tropical tropopause layer TTL, *J. Geophys. Res.*, 117,  
840 D09303, doi:10.1029/2011JD017267, 2012.

841 Ploeger, F., G. Günther, P. Konopka, S. Fueglistaler, R. Müller, C. Hoppe, A. Kunz, R. Spang,  
842 J.-U. Grooß, and M. Riese, Horizontal water vapor transport in the lower stratosphere  
843 from subtropics to high latitudes during boreal summer, *J. Geophys. Res. Atmos.*, 118,  
844 8111–8127, doi:10.1002/jgrd.50636, 2013.

845 Powell K., Vaughan M., Winker D., K. M. Lee, Pitts M., Trepte C.: CALIPSO Data Product  
846 Catalog, Release 3.6, Document No: PC-SCI-503, 2013.

847 Rahul P. R. C., Bhawar R. L., Ayantika D. C., Panicker A. S., Safai P. D., Tharaprabhakaran V.,  
848 Padmakumari B., and Raju M. P., Double blanket effect caused by two layers of black  
849 carbon aerosols escalates warming in the Brahmaputra River Valley, *Scientific Reports*,  
850 4, 3670, DOI: 10.1038/srep03670, 2014.

857 Rajagopalan, B., and P. Molnar, Signatures of Tibetan Plateau heating on Indian summer  
858 monsoonrainfall variability, *J. Geophys. Res. Atmos.*, 118, 1170–1178,  
859 doi:10.1002/jgrd.50124, 2013.

860 Ramanathan, V., Crutzen, P. J., Lelieveld, J., Mitra, A. P., Althausen,D., Anderson, J., Andreae,  
861 M. O., Cantrell, W., Cass,G. R., Chung, C. E., Clarke, A. D., Coakley, J. A., Collins,W.  
862 D.,Conant, W. C., Dulac, F., Heintzenberg, J., Heymsfield, A. J.,Holben, B., Howell, S.,  
863 Hudson, J., Jayaraman, A., Kiehl, J. T.,Krishnamurti, T. N., Lubin, D., McFarquhar, G.,  
864 Novakov, T.,Ogren, J. A., Podgorny, I. A., Prather, K., Priestley, K., Prospero,J. M.,  
865 Quinn, P. K., Rajeev, K., Rasch, P., Rupert, S., Sadourny,R., Satheesh, S. K., Shaw, G.  
866 E., Sheridan, P., and Valero, F. P. J.: Indian Ocean Experiment: An integrated analysis of  
867 the climateforcing and effects of the great Indio-Asian haze, *J. Geophys.Res.*, 106,  
868 28371–28398, 2001.

869 Ramanathan, V., Crutzen, P. J., Kiehl, J. T. and Rosenfeld, D., Aerosols, Climate, and the  
870 Hydrological Cycle , *Science* 294, 2119–2124, doi: 10.1126/science.1064034, 2001b.

871 Ramanathan V. Crutzen P. J.: New directions: Atmospheric brown “clouds”, *Atmos.*  
872 *Environ.* 37:4033–4035, doi:10.1016/S1352-2310(03)00536-3, 2003.

873 Ramanathan, V. and Carmichael, G.: Global and regional climate changes due to black carbon,  
874 *Nat. Geosci.*, 1, 221–227, doi:10.1038/ngeo156, 2008.

875 Ramaswamy, V., Ramanathan, V. Solar absorption of cirrus clouds and the maintenance of the  
876 tropical upper troposphere thermal structure. *J. Atmos. Sci.* 46, 2293–2310, doi:  
877 [http://dx.doi.org/10.1175/1520-0469\(1989\)046<2293:SABCCA>2.0.CO;2](http://dx.doi.org/10.1175/1520-0469(1989)046<2293:SABCCA>2.0.CO;2) 1989.

878 Randall, D.A., Harshovardan, Dazlich, D.A., Corsetti, T.G. Interactions among radiation,  
879 convection, and large-scale dynamics in a general circulation model. *J. Atmos. Sci.* 46,  
880 1943–1970, doi:10.1175/1520-0469(1989)046<1943:IARCAL>2.0.CO;2, 1989.

881 Randel,W. J. and Park, M.: Deep convective influence on the Asian summer monsoon  
882 anticyclone and associated tracer variability observed with Atmospheric Infrared Sounder  
883 (AIRS), *J. Geophys. Res.*, 111, D12314, doi:10.1029/2005JD006490, 2006.

884 Randel, W. J., Park, M., Emmons, L., Kinnison, D., Bernath, P., Walker, K. A., Boone, C., and  
885 Pumphrey H.: Asian monsoon transport of pollution to the stratosphere, *Science*, 328,  
886 611–613, doi: 10.1126/science.1182274, 2010.

887 Rosenfield, D., Suppression of rain and snow by urban and industrial air pollution, *Science*, 287,  
888 1793–1796, doi: 10.1126/science.287.5459.1793,2000.

889 Satheesh, S. K. and Ramanathan, V.: Large differences in tropical aerosol forcing at the top of  
890 the atmosphere and Earth’s surface, *Nature*, 405, 60–63, doi:10.1038/35011039, 2000.

891 Schultz, M. G., Heil, A., Hoelzemann, J. J., Spessa, A., Thonicke, K., Goldammer, J., Held, A.  
892 C., Pereira, J. M., and van het Bolscher, M.: Global wildland fire emissions from 1960 to  
893 2000, *Global Biogeochem. Cyc.*, 22, GB2002, doi:10.1029/2007GB003031,2008.

894 Solomon, S., Qin, D., Manning, M., Chen, Z., Marquis, M., Averyt, K.B., Tignor M. and Miller,  
895 H. L., Contribution of Working Group I to the Fourth Assessment Report of the  
896 Intergovernmental Panel on Climate Change, Cambridge University Press, Cambridge,  
897 United Kingdom and New York, NY, USA. 2007.

898 Sreekanth, V., Niranjana, K. and Madhavan, B. L., Radiative forcing of black carbon over eastern  
899 India, *Geophys. Res. Lett.*, 34, L17818, doi:10.1029/2007GL030377, 2007.

900 Stephens, G. L., Vane, D.G., Taneeli, S., Im, E., Durden, S., Rockey, M., Reinke, D., Partain, P.,  
901 Mace, G.G., Austin, R., Ecuyet, T.L., Haynes, J., Lebsock, M., Suzuki, K., Waliser, D.,  
902 Wu, D., Kay, J., Gettelman, A., Wang, Z., Marchand, R.: CloudSat mission: Performance  
903 and early science after the first year of operation, *J. Geophys. Res.*, 113, D00A18,  
904 doi:10.1029/2008JD009982,2008.

905 Stevens, B., Giorgetta M., Esch M., Mauritsen T., Crueger T., Rast S., Salzmann M., Schmidt H.,  
906 Bader J., Block K., Brokopf R., Fast I., Kinne S., Kornbluh L., Lohmann U., Pincus R.,  
907 Reichler T., and Roeckne E., Atmospheric component of the MPI-M Earth System  
908 Model: ECHAM6, *J. of Advances in Modeling Earth Systems*. **5**, 1–27,  
909 doi:10.1002/jame.20015, 2013.

910 Stier, P., Feichter, J., Kinne, S., Kloster, S., Vignati, E., Wilson, J., Ganzeveld, L., Tegen, I.,  
911 Werner, M., Balkanski, Y., Schulz, M., Boucher, O., Minikin, A. and Petzold, A.: The  
912 aerosol-climate model ECHAM5-HAM, *Atmos. Chem. Phys.*, **5**, 1125-1156,  
913 doi:10.5194/acp-5-1125-2005, 2005.

914 Streets, D. G., Yan, F., Chin, M., Diehl, T., Mahowald, N., Schultz, M., Wild, M., Wu, Y., and  
915 Yu, C.: Anthropogenic and natural contributions to regional trends in aerosol optical  
916 depth, 1980–2006, *J. Geophys. Res.*, 114, D00D18, doi:10.1029/2008jd011624, 2009.

917 Takahashi, H. G.: Seasonal and diurnal variations in rainfall characteristics over the tropical  
918 Asian monsoon region using TRMM-PR data. SOLA, 12A, 22–27, doi:10.2151/  
919 sola.12A-005, 2016.

920 Tegen, I., Harrison, S. P., Kohfeld, K., Prentice, I. C., Coe, M., and Heimann, M.: Impact of  
921 vegetation and preferential source areas on global dust aerosol: Results from a model  
922 study, *J. Geophys. Res.-Atmos.*, 107, 4576, doi:10.1029/2001JD000963, 2002.

923 Thomason, L. W. and Vernier, J.P.: Improved SAGE II cloud/aerosol categorization and  
924 observations of the Asian tropopause aerosol layer: 1989–2005, *Atmos. Chem. Phys.*, 13,  
925 4605–4616, doi:10.5194/acp-13-4605-2013, 2013.

926 Tobo, Y., Iwasaka, Y., Yu Shi, G., Kim, Y. S., Ohashi, T, Tamura, K. and Zhang, D.: Balloon-  
927 borne observations of high aerosol concentrations near the summertime tropopause over  
928 the Tibetan Plateau, *Atmospheric Research*, 84, 233–  
929 241, doi:10.1016/j.atmosres.2006.08.003, 2007.

931 Tripathi, S.N., Srivastava, A.K., S. Dey, S., Satheesh, S.K., Krishnamoorthy, K.: The vertical  
932 profile of atmospheric heating rate of black carbon aerosols at Kanpur in northern India,  
933 *Atmos. Environ.*, 41, 6909–6915, doi: <http://dx.doi.org/10.1016/j.atmosenv.2007.06.032>,  
934 2007.

938 Van der Werf, G. R., Randerson, J.T., Giglio, L., Collatz, G.J., Kasibhatla, P.S., Arellano A.F.:  
939 Interannual variability in global biomass burning emissions from 1997 to 2004, *Atmos.*  
940 *Chem. Phys.*, 6, 3423–3441, doi:10.5194/acp-6-3423-2006, 2006.

941 Vernier, J. P., L. W. Thomason, and J. Kar.: CALIPSO detection of an Asian tropopause aerosol  
942 layer, *Geophys. Res. Lett.*, 38, L07804, doi:10.1029/2010GL046614, 2011.

943 Vernier, J.P., Fairlie, T.D., Natarajan, M., Wienhold, F.G., Bian, J., Martinsson, B.G.,  
944 Crumeyrolle, S., Thomason, L.W., Bedka, K.M.: Increase in upper tropospheric and  
945 lower stratospheric aerosol levels and its potential connection with Asian pollution, *J.*  
946 *Geophys. Res. Atmos.*, 120, 1608–1619, doi:10.1002/2014JD022372, 2015.

947 Vignati, E., Wilson, J., and Stier, P.: An efficient size-resolved aerosol microphysics module for  
948 large-scale aerosol transport models, *J. Geophys. Res.*, 109, D22202,  
949 doi:10.1029/2003JD004485, 2004.

950 Vиноj V, Rasch P. J., Wang H., Yoon J-H, Ma P-L, Landu K. and Singh B., Short-term  
951 modulation of Indian summer monsoon rainfall by West Asian dust, *Nature Geoscience*  
952 7, 308–313, doi:10.1038/ngeo2107, 2014.

953 Vogel B., Pan L. L., Konopka P., Günther G., Müller R., Hall W., Campos T., Pollack T.,  
954 Weinheimer A., Wei J., Atlas E. L. and Bowman K.P., Transport pathways and  
955 signatures of mixing in the extratropical tropopause region derived from Lagrangian  
956 model simulations, *J. Geophys. Res.*, 116, D05306, doi:10.1029/2010JD014876, 2011.

957 Vogel B., Günther G., Müller R., Grooß J.-U., and Riese M., Impact of different Asian source  
958 regions on the composition of the Asian monsoon anticyclone and of the extratropical  
959 lowermost stratosphere, *Atmos. Chem. Phys.*, 15, 13699–13716, doi:10.5194/acp-15-  
960 13699-2015, 2015.

961 Wang, B. and Linho, Rainy Season of the Asian–Pacific Summer Monsoon, *Journal of Climate*,  
962 15, 386-398, [http://dx.doi.org/10.1175/1520-0442\(2002\)015<0386:RSOTAP>2.0.CO;2](http://dx.doi.org/10.1175/1520-0442(2002)015<0386:RSOTAP>2.0.CO;2)  
963 2002.

964 Wang, C. A modeling study on the climate impacts of black carbon aerosols, *J. Geophys. Res.*,  
965 109, D03106, doi:10.1029/2003JD004084, 2004.

966 Wang, C., Impact of direct radiative forcing of black carbon aerosols on tropical convective  
967 precipitation, *Geophys. Res. Lett.*, 34, L05709, doi:10.1029/2006GL028416, 2007.

968 Wang, C., Kim, D., Ekman, A. M. L., Barth, M. C and Rasch, P. J.: Impact of anthropogenic  
969 aerosols on Indian summer monsoon, *Geophys. Res. Lett.*, 36, L21704,  
970 doi:10.1029/2009GL040114, 2009.

971 Winiger P., Andersson A., Eckhardt S., Stohl A. and Gustafsson O.: The sources of atmospheric  
972 black carbon at a European gateway to the Arctic, *Nature Communications*, 7, 12776,  
973 doi: 10.1038/ncomms12776, 2016.

974 Winker, D., Pelon, J., Coakley, J., Ackerman, S., Charlson, R., Colarco, P., Flamant, P., Fu, Q.,  
975 Hoff, R., Kittaka, C., Kubar, T.L., Le Treut, H., McCormick, M.P., Mégie, G., Poole, L.,  
976 Powell, K., Trepte, C., Vaughan, M.A., Wielicki, B.A.: THE CALIPSO MISSION A  
977 Global 3D View of Aerosols and Clouds. *Bull Amer Meteorol Soc.*, 91, 1211-1229, doi:  
978 <http://dx.doi.org/10.1175/2010bams3009.1>, 2010.

979 Wu G., and Zhang Y. : Tibetan Plateau forcing and timing of the monsoon onset over South Asia  
980 and South China Sea, *Monthly Weather Review*, 126, 913–927, doi:  
981 [http://dx.doi.org/10.1175/1520-0493\(1998\)126<0913:tpfatt>2.0.co;2](http://dx.doi.org/10.1175/1520-0493(1998)126<0913:tpfatt>2.0.co;2), 1998.

982 Xie, P., Yatagai, A., Chen, M., Hayasaka, T., Fukushima, Y., Liu, C., Yang, S.: A Gauge-  
983 Based Analysis of Daily Precipitation over East Asia, *Journal of Hydrometeorology*, doi:  
984 10.1175/JHM583.1, 2007.

985 Xiong, X., Houweling, S., Wei, J., Maddy, E., Sun, F., and Barnett, C.: Methane plume over  
986 south Asia during the monsoon season: satellite observation and model simulation,  
987 *Atmos. Chem. Phys.*, 9, 783–794, doi:10.5194/acp-9-783-2009, 2009.

988 Yanai, M., Li, C., Song, Z.: Seasonal heating of the Tibetan Plateau and its effects on the  
989 evolution of the Asian summer monsoon, *J Meteor Soc Japan*, 70, 189–221, 1992.

990 Yu, P., Toon, O.B., Neely, R.R., Martinsson, B.G., Brenninkmeijer, C.A.M.: Composition and  
991 physical properties of the Asian Tropopause Aerosol Layer and the North American  
992 Tropospheric Aerosol Layer, *Geophys. Res. Lett.*, 42, 2540–2546, doi:10.1002/, 2015.

993 Zhang K., D. O'Donnell, J. Kazil, P. Stier, S. Kinne, U. Lohmann, S. Ferrachat, B. Croft, J.  
994 Quaas, H, Wan, S. Rast, and J. Feichter 2012.: The global aerosol-climate model  
995 ECHAM-HAM, Version 2: Sensitivity to improvements in process representations,  
996 *Atmos. Chem. Phys.*, 12, 8911-8949, doi:10.5194/acp-12-8911-2012, 2012.

997 Zhang L., Henze D. K., Grell G. A., Carmichael G. R., Bousserez N., Zhang Q., Torres O., Ahn  
998 C., Lu Z., Cao J., and Mao Y.: Constraining black carbon aerosol over Asia using OMI  
999 aerosol absorption optical depth and the adjoint of GEOS-Chem, *Atmos. Chem. Phys.*,  
1000 15, 10281–10308, doi:10.5194/acp-15-10281-2015, 2015.

1001

1002 Table-1: ECHAM6 HAM simulated total (shortwave and long wave) radiative forcing ( $W m^{-2}$ )  
1003 along with two standard deviation values averaged over the TP and Indo-Gangetic Plains ( $80^{\circ}E$   
1004  $-110^{\circ}E$ ;  $15^{\circ}N$  - $35^{\circ}N$ ) region.

Model run	TOA	Surface	Atmosphere
Demiss-CTRL	$+0.37 \pm 0.26$	$-4.74 \pm 1.42$	$+5.11 \pm 0.83$
DBConly-CTRL	$+0.31 \pm 0.25$	$-4.20 \pm 0.81$	$+4.52 \pm 0.38$
DOConly-CTRL	$-0.51 \pm 0.32$	$-1.96 \pm 0.95$	$+1.45 \pm 0.49$

1005  
1006  
1007  
1008  
1009  
1010  
1011  
1012  
1013  
1014  
1015  
1016  
1017  
1018



1019  
1020  
1021  
1022  
1023  
1024  
1025  
1026  
1027  
1028  
1029  
1030  
1031  
1032  
1033  
1034  
1035  
1036  
1037  
1038  
1039  
1040  
1041  
1042  
1043  
1044  
1045  
1046  
1047  
1048  
1049  
1050  
1051  
1052  
1053  
1054  
1055  
1056  
1057  
1058  
1059  
1060  
1061  
1062  
1063

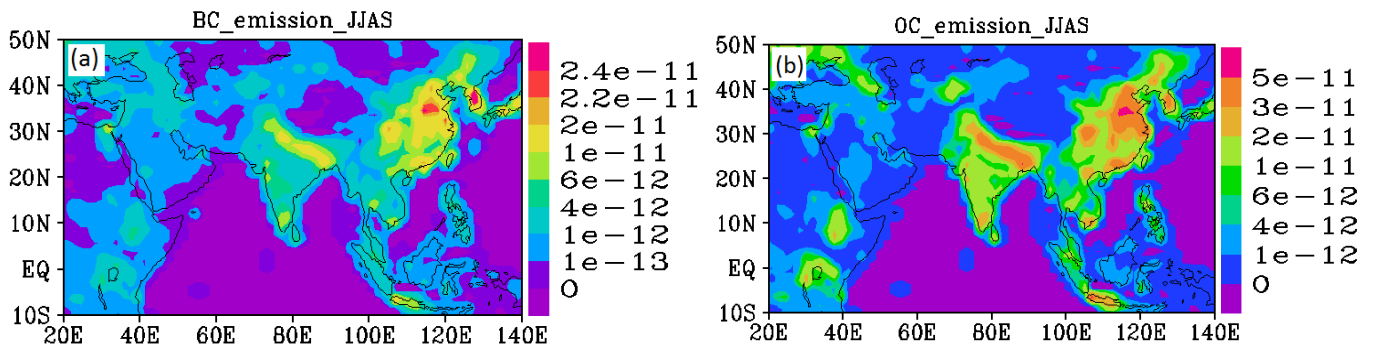
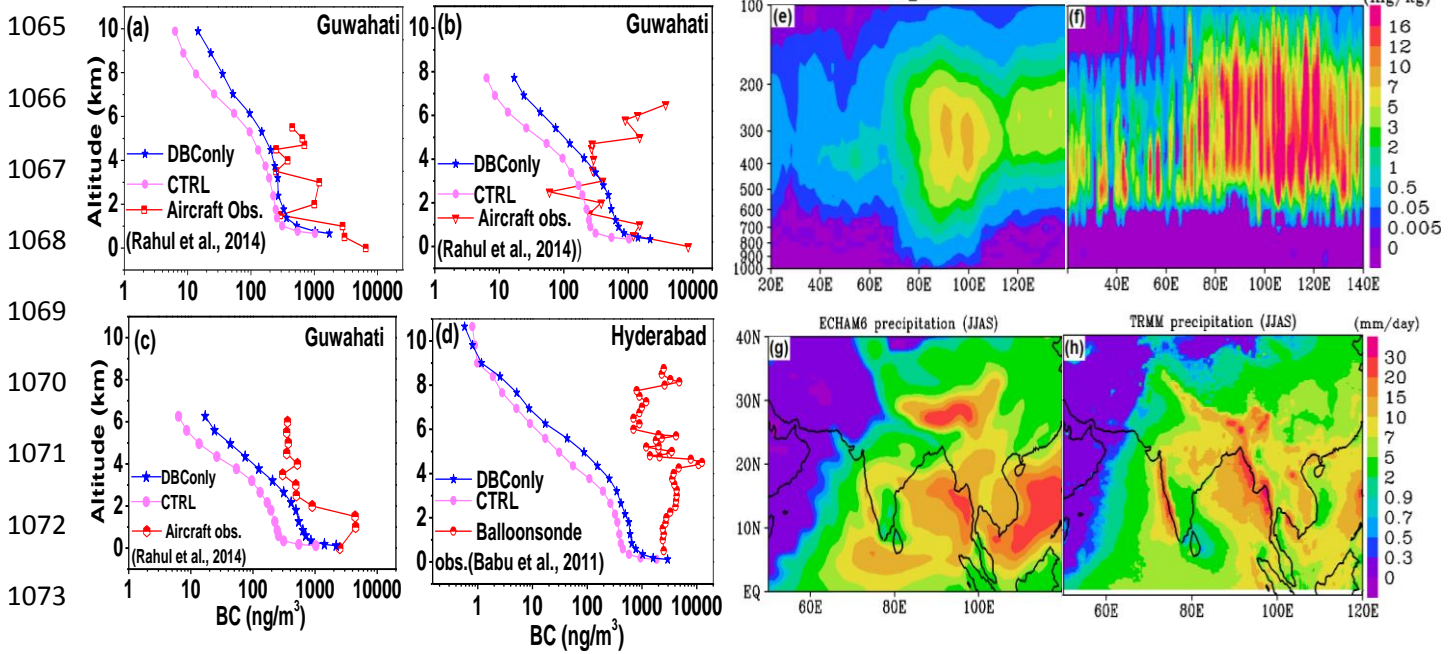


Figure1: Distribution of emission mass flux ( $\text{kg m}^{-2} \text{s}^{-1}$ ) averaged for the monsoon season (June-September) for (a) BC and (b) OC aerosols.

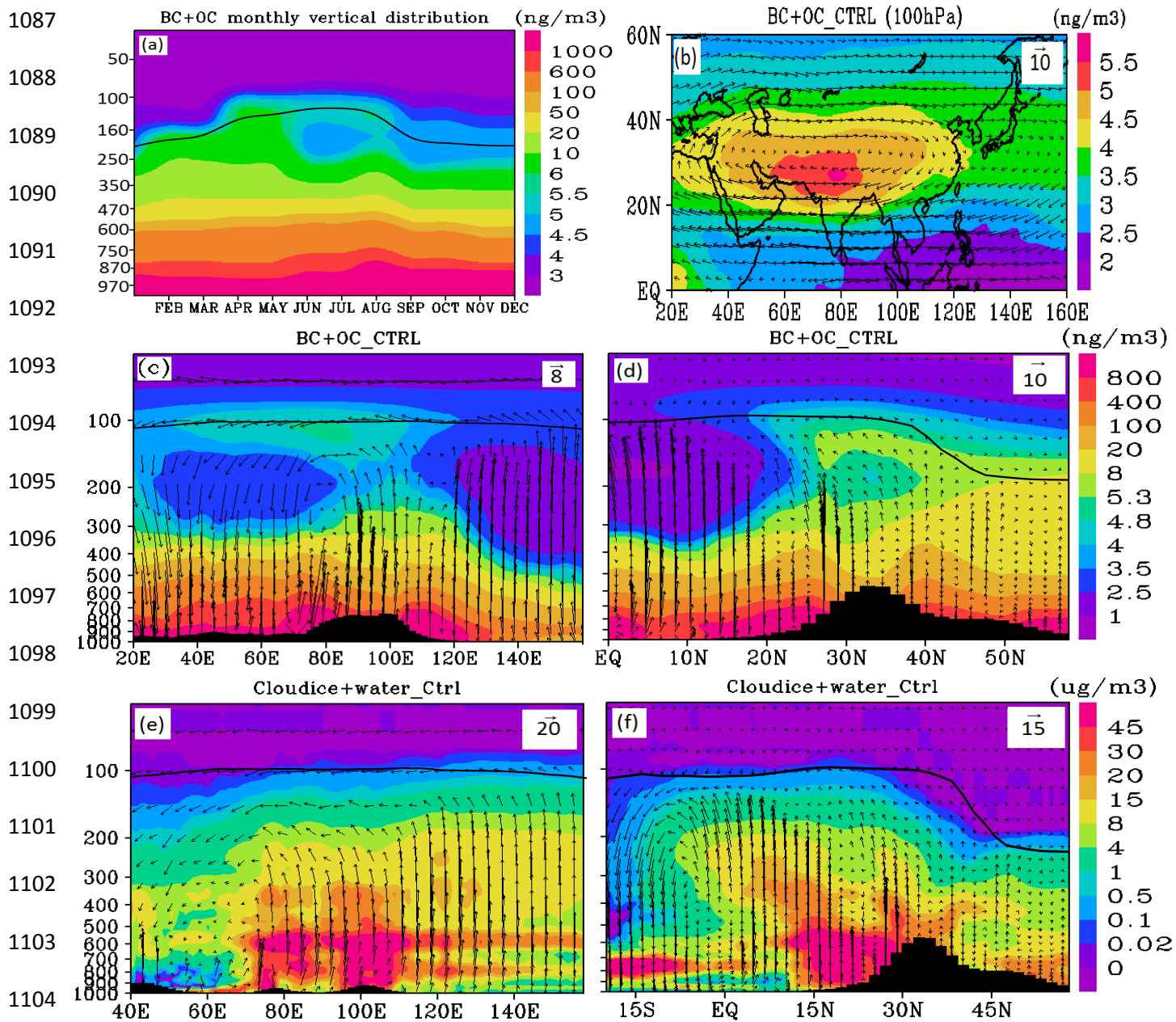
1064



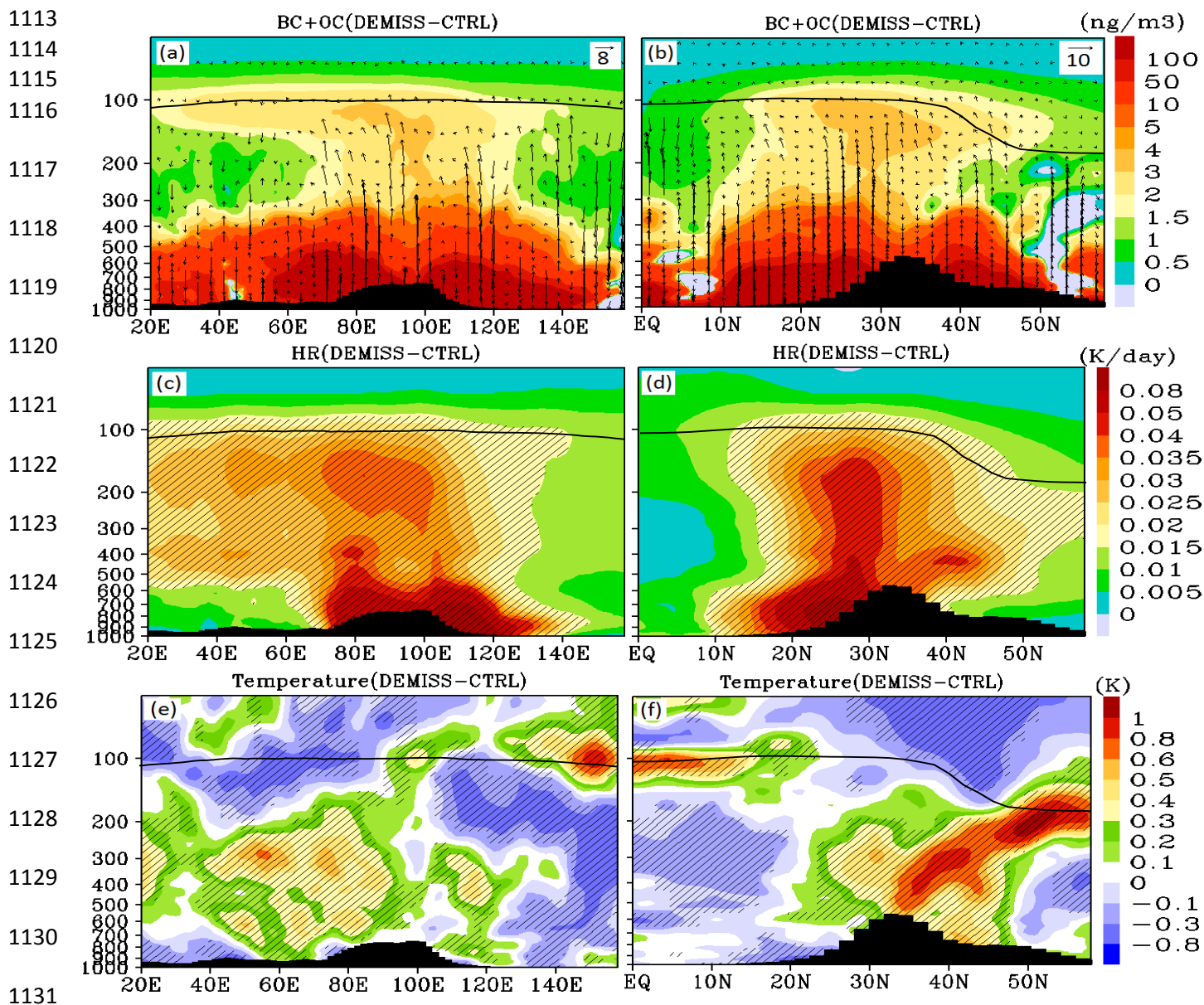
1074

1075 Figure 2: Vertical distribution of BC aerosols ( $\text{ng m}^{-3}$ ) (a) aircraft measurements on 30 August  
1076 2009 at Guwahati ( $26^{\circ}11'N$ ,  $91^{\circ}44'E$ ) (Rahul et al., 2014), CTRL, DBCOnly simulations for the  
1077 month of August extracted at a grid centered at Guwahati, (b) same as (a) but observations for 4  
1078 September 2009 and simulations for the month of September, (c) same as (a) but for observations  
1079 on 6 September 2009 and simulations for the month of September, (d) Balloonborne  
1080 measurement on 17 March 2010 at Hyderabad ( $17^{\circ}48'N$ ,  $78^{\circ}40'E$ ) (Babu et al., 2011) and  
1081 CTRL, DBCOnly simulations for the month of March at a grid centred at Hyderabad. Seasonal  
1082 mean distribution of cloud ice mass mixing ratio ( $\text{mg kg}^{-1}$ ) averaged for  $20^{\circ}N$ - $40^{\circ}N$  (e) CTRL  
1083 simulation, (f) CloudSat and CALIPSO combined 2C-ICE L3 for the years 2007-2010. Seasonal  
1084 mean precipitation ( $\text{mm day}^{-1}$ ) obtained from (g) CTRL simulation, (h) TRMM averaged for  
1085 period 1998-2005.

1086

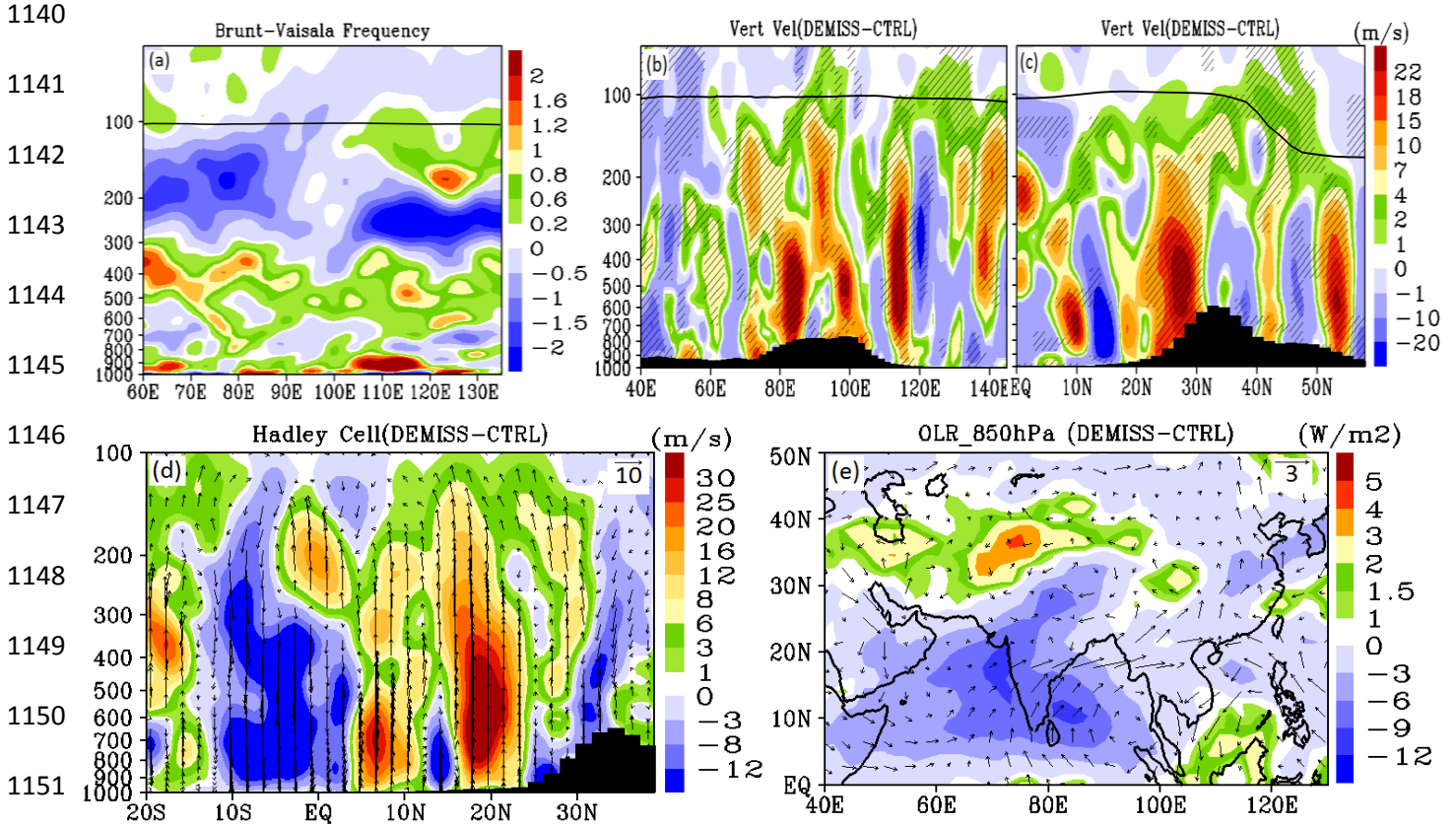


1105 Figure 3: Distribution of BC and OC aerosols ( $\text{ng m}^{-3}$ ) together from CTRL simulations (a)  
 1106 monthly variations averaged for the region  $70^{\circ}\text{E} - 120^{\circ}\text{E}$ ,  $25^{\circ}\text{E} - 45^{\circ}\text{E}$ , Seasonal mean  
 1107 distribution of BC and OC aerosols ( $\text{ng m}^{-3}$ ) together from CTRL simulations (b) at 100 hPa, (c)  
 1108 averaged for  $15^{\circ}\text{N} - 35^{\circ}\text{N}$ , (d) averaged for  $80^{\circ}\text{E} - 110^{\circ}\text{E}$ , seasonal mean distribution of cloud  
 1109 ice+cloud water ( $\mu\text{g m}^{-3}$ ) from CTRL simulations (e) averaged for  $10^{\circ}\text{N} - 25^{\circ}\text{N}$ , (f) averaged for  
 1110  $80^{\circ}\text{E} - 110^{\circ}\text{E}$ . Black arrows indicate wind vectors. The vertical velocity field has been scaled by  
 1111 1000. The black line represents the tropopause. In Figs. (a), (c), (d), (e), (f) tropopause is  
 1112 averaged over the same region where field parameter is averaged.



1132 Figure 4: Distribution of anomalies (Demiss - CTRL), of BC and OC aerosols ( $\text{ng m}^{-3}$ ) together  
 1133 averaged for the monsoon season (a) averaged for  $15^\circ\text{N} - 35^\circ\text{N}$  (b) averaged for  $80^\circ\text{E} - 110^\circ\text{E}$ ,  
 1134 Black arrows indicate wind vectors (the vertical velocity field has been scaled by 1000), (c) and  
 1135 (d) same as (a) and (b) but for heating rate anomalies ( $\text{K day}^{-1}$ ). Distribution of anomalies in  
 1136 temperature ( $\text{K}$ ) (e) averaged for  $15^\circ\text{N} - 35^\circ\text{N}$ , (f) averaged for  $80^\circ\text{E} - 110^\circ\text{E}$ . The black line  
 1137 represents the tropopause. The tropopause is averaged over  $15^\circ\text{N} - 35^\circ\text{N}$  for Figs. (a), (c), (e) and  
 1138 over  $80^\circ\text{E} - 110^\circ\text{E}$  for Figs. (b), (d) and (f). Black hatched lines in Figs. (c), (d), (e) and (f) indicate  
 1139 99% confidence level.





1152

1153 Figure 5: Vertical distribution of anomalies (Demiss-CTRL) averaged for the monsoon season  
 1154 (a) square of Brunt Väisälä frequency (per sec\*1E-5) averaged over 25°N-40°N, (b) vertical  
 1155 velocities (m s<sup>-1</sup>) averaged for 15°N-35°N, (c) same as (b) but averaged for 80°E-110°E, (d)  
 1156 difference in the meridional circulation averaged for 70°E-90°E. Black arrows indicate wind  
 1157 vectors, (e) Distribution of OLR (shaded) (W m<sup>-2</sup>) and winds at 850 hPa (m s<sup>-1</sup>). In Figs (b)-(d)  
 1158 the vertical velocity field has been scaled by 1000 and the thick black line shows the tropopause.  
 1159 Black hatched lines in Figs (b) and (c) indicate 99% confidence level.

1160

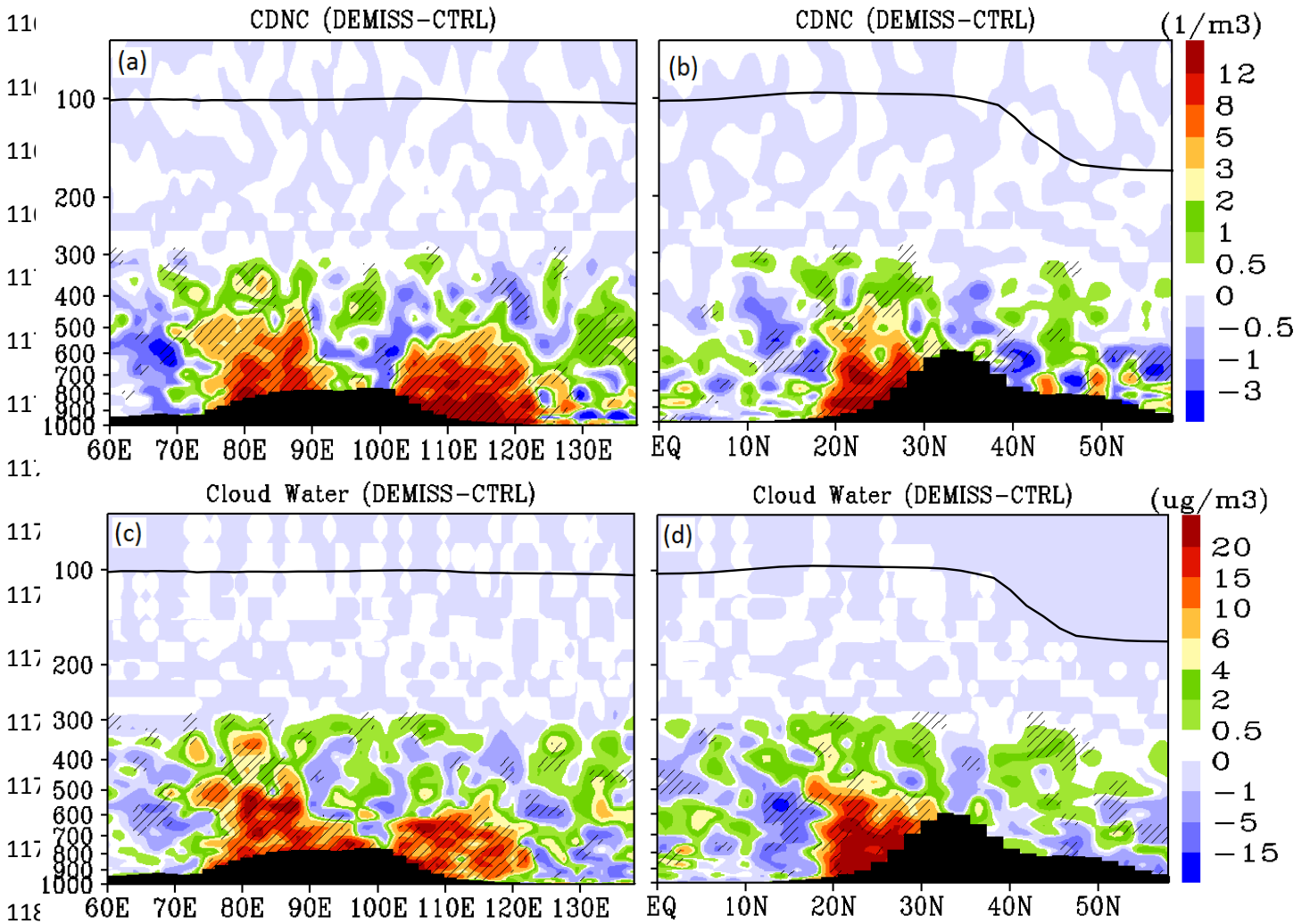
1161

1162

1163

1164

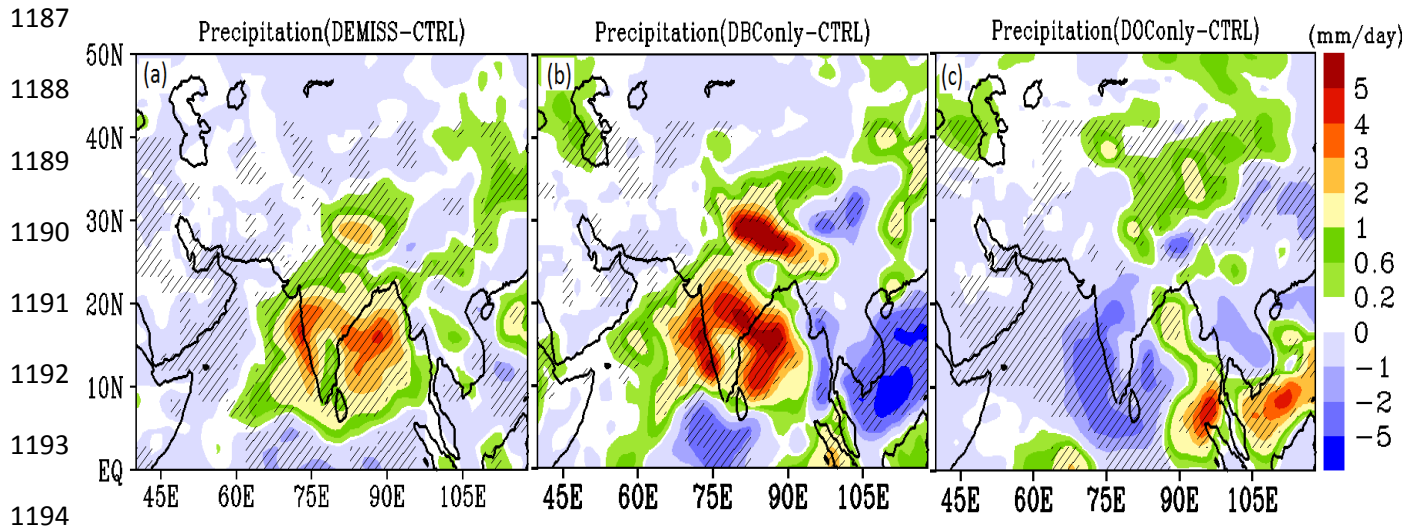
1165



1181 Figure 6: Distribution of anomalies (Demiss-CTRL) averaged for the monsoon season (a) CDNC  
1182 ( $\text{m}^{-3}$ ) averaged for  $15^{\circ}\text{N}$ - $35^{\circ}\text{N}$ , (b) same as (a) but averaged for  $80^{\circ}\text{E}$ - $110^{\circ}\text{E}$ , (c) cloud water ( $\mu\text{g}$   
1183  $\text{m}^{-3}$ ) averaged for  $15^{\circ}\text{N}$ - $35^{\circ}\text{N}$ , (d) same as (c) but averaged over  $80^{\circ}\text{E}$ - $110^{\circ}\text{E}$ . Black hatched  
1184 lines in Figs. a-d indicate 99% confidence level.

1185

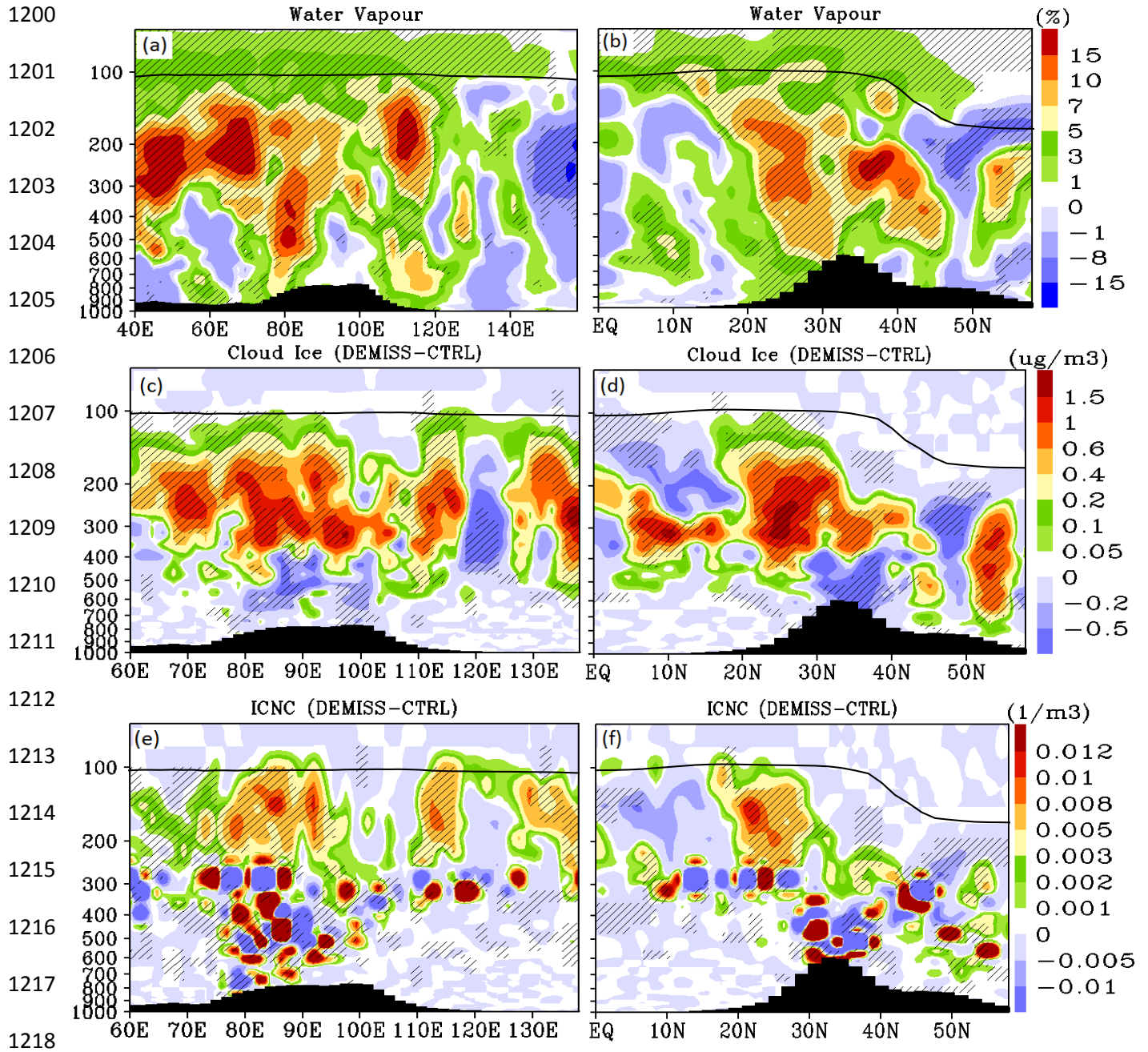
1186



1195

1196 Figure 7: Distribution of anomalies in precipitation ( $\text{mm day}^{-1}$ ) averaged for the monsoon season  
 1197 obtained from (a) Demiss-CTRL, (b) DBConly-CTRL, (C) DOConly-CTRL. Black hatched lines  
 1198 indicate 99% confidence level.

1199



1219 Figure 8: Distribution of anomalies (Demiss-CTRL) averaged for the monsoon season, (a) water  
 1220 vapour (%) averaged over 15°N - 35°N, (b) same as (a) but averaged over 80°E - 110°E, (c) and  
 1221 (d) same as (a) and (b) but for cloud ice ( $\mu\text{g}/\text{m}^3$ ) and (e) and (f) for ice crystal number  
 1222 concentration (ICNC) ( $\text{m}^{-3}$ ). The thick black line shows the tropopause while black hatched lines  
 1223 indicate 99% confidence level. The tropopause is averaged over 15°N - 35°N for Figs. (a), (c), (e)  
 1224 and over 80°E - 110°E for Figs. (b), (d) and (f).